Journal of
Water & Climate Change

Journal of Water and Climate Change Vol 15 No 1, 209 doi: 10.2166/wcc.2023.656

Impacts of hydroclimate change on climate-resilient agriculture at the river basin management

Chiranjit Singha [a], Satiprasad Sahoo [b], Ajit Govind [b], Biswajeet Pradhan [c,d], Shatha Alrawashdeh [e], Taghreed Hamdi Aljohani [f], Hussein Almohamad [g], Abu Reza Md Towfiqul Islam [h,i] and Hazem Ghassan Abdo [j,*]

[a] Department of Agricultural Engineering, Institute of Agriculture, Visva-Bharati (A Central University), Sriniketan, Birbhum 731236, India
[b] International Center for Agricultural Research in the Dry Areas (ICARDA), 2 Port Said, Victoria Sq, Ismail El-Shaaer Building, Maadi, Cairo 11728, Egypt
[c] Centre for Advanced Modelling and Geospatial Information Systems (CAMGIS), School of Civil and Environmental Engineering, Faculty of Engineering and IT, University of Technology Sydney, Sydney, NSW 2007, Australia
[d] Earth Observation Centre, Institute of Climate Change, Universiti Kebangsaan Malaysia, Bangi, Selangor43600 UKM, Malaysia
[e] Department of Geography, Faculty of Art, Al-Hussein Bin Talal university, Ma'an, Jordan
[f] Geography Department, Faculty of Arts and Humanities, Taibah University, Medina, Saudi Arabia
[g] Department of Geography, College of Arabic Language and Social Studies, Qassim University, Buraydah 51452, Saudi Arabia
[h] Department of Disaster Management, Begum Rokeya University, Rangpur 5400, Bangladesh
[i] Department of Development Studie, Daffodil International University, Dhaka 1216, Bangladesh
[j] Geography Department, Faculty of Arts and Humanities, Tartous University, Tartous, Syria
*Corresponding author. E-mail: hazemabdo@tartous-univ.edu.sy

CS, 0000-0003-1204-1750; HGA, 0000-0001-9283-3947

ABSTRACT

This paper focuses on exploring the potential of Climate resilient agriculture (CRA) for river basin-scale management. Our analysis is based on long-term historical and future climate and hydrological datasets within a GIS environment, focusing on the Ajoy River basin in West Bengal, Eastern India. The standardized anomaly index (SAI) and slope of the linear regression (SLR) methods were employed to analyse the spatial pattern of the climate variables (precipitation, T_{max} and T_{min}) and hydrological variables (actual evapotranspiration (AET), runoff (Q), vapor pressure deficit (VPD), potential evapotranspiration (PET), and climate water deficit (DEF)) using the TerraClimate dataset spanning from 1958 to 2020. Future climate trend analysis spanning 2021 to 2050 was conducted using the CMIP6 based GCMs (MIROC6 and EC-Earth3) dataset under shared socio-economic pathway (SSP2-4.5, SSP5-8.5 and historical). For spatiotemporal water storage analysis, we relied on Gravity Recovery and Climate Experiment (GRACE) from the Center for Space Research (CSR) and the Jet Propulsion Laboratory (JPL) data, covering the period from 2002 to 2021. Validation was performed using regional groundwater level data, employing various machine learning classification models. Our findings revealed a negative precipitation trend (approximately −0.04 mm/year) in the southern part, whereas the northern part exhibited a positive trend (approximately 0.10 mm/year).

Key words: agricultural adaptability, climate change, climate-resilient agriculture, food security, hydroclimatic change

HIGHLIGHTS

- The slope of the linear regression method was employed for the spatial distribution of the climatic and hydrological conditions (1958–2020).
- Future climate trend analysis (2021–2100) has been executed through the CMIP6 (MIROC6 and EC-Earth3) SSP245, SSP585 and historical dataset.
- A novel ensemble boosting machine learning algorithm was used for the validation of groundwater level.

GRAPHICAL ABSTRACT

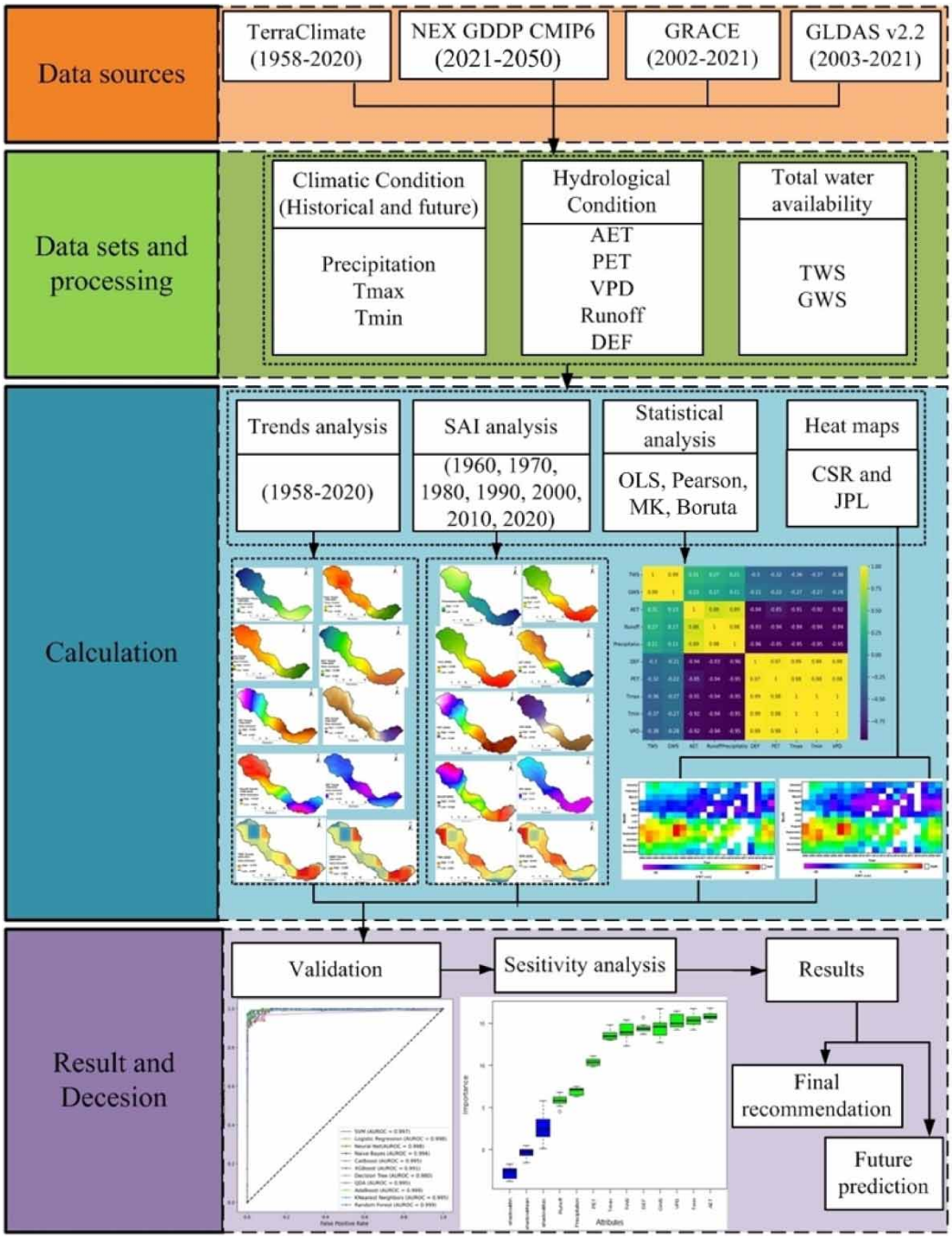

1. INTRODUCTION

Climate change is a major global concern for agricultural water management, it significantly threatening agricultural productivity (Guptha *et al.* 2022). The Intergovernmental Panel on Climate Change (IPCC) reported that climate change refers to long-term change in climatic patterns. These changes are usually observed in the annual or seasonal variations of the climate (IPCC 2013). Moreover, the IPCC's fifth assessment report (AR5) also identified different climate-resilient pathways, e.g., mitigation and adaptation strategies (Werners *et al.* 2021). These pathways aim to provide a comprehensive view of the diverse impacts of climate change on both natural and anthropogenic systems, including rural poverty, the environment, and

livelihoods (Sam *et al.* 2020; Pushpanjali *et al.* 2021). It is estimated that, around half of the world's population, around 8 billion people, may experience severe water scarcity at some point during the year due to a combination of non-climatic and climatic factors (IPCC 2019). Climate change is contributing to the likelihood of severe and prolonged droughts and floods in various regions with high level of confidence (Pekel *et al.* 2016; Singha *et al.* 2022). The Fifth AR5 emphasizes that natural disasters such as floods and droughts pose a significant threat to agricultural production, highlighting climate-resilient strategies as a top priority for ensuring food security (Caretta *et al.* 2022). The over-exploitation of groundwater for agricultural, domestic, and industrial purposes has accelerated the depletion of water storage worldwide (Arneth *et al.* 2019).

In the face of these challenges, both private and public organizations recognize adaptation a crucial measure to combat with the effects of climate change on agriculture and water security-related issues (Rusia *et al.* 2018). Neglecting the need for measures addressing climate change's effects on the water cycle could lead to a projected decrease in global gross domestic product (GDP) by 2050, particularly in low- and middle-income countries (Acevedo *et al.* 2020). Thusway, climate-resilient agriculture (CRA) practices help farmers to manage natural hazards and mitigate the associated effects of climate change. This domain of the CRA approach involves developing new strategies and practices to enhance the productivity of the farm and land, reduce greenhouse gas emissions (GHGs) from agriculture, and increase farmers' incomes (Singha *et al.* 2020). These practices also contribute to climate adaptability, poverty reduction, and food security amid changing climate scenarios with the Sustainable Development Goals (SDGs) specially with numbers 1, 2, and 13 (Singh 2020). Recent studies showed that, climate change's impact on hydrology at the river basin scale has been assessed using various hydrological models under CMIP5 and CMIP6 scenarios within the CRA domain (Karan *et al.* 2022). Amiri & Gocic (2023); Milan & Amiri (2023) showed the long-term (1946–2019) water balance scenario through the various rainfall indices namely the standardized anomaly index (SAI), the standardized precipitation index (SPI), the rainfall anomaly index (RAI), the China Z index (CZI), the percent of normal precipitation (PNP), and the modified China Z index (MCZI) over Serbia. Another study of Amiri & Gocic (2021) showed the precipitation concentration degree (PCD), the precipitation concentration index (PCI), the precipitation concentration period (PCP) and the seasonal PCI (SPCI), were analyzed using long-term precipitation data (1946–2019) for climate change applicability in Serbia. Topographical variation was directly correlated with the precipitation variability. The maximum correlations are also found between the for latitude, and PCD and longitude and the summer PCI at 0.73, and 0.75, respectively. Milan & Amiri (2023) estimated the precipitation trend analysis through the polynomial fit equation in northwest Iran. The outcome showed that southwest part had incremental trend in the study period (1991–2010).

The use of geospatial technology has both potential advantages and indirect implications for the establishment of a long-term CRA framework. Various studies have used different multisensory remote sensing (RS) data sources, including the Global Land Data Assimilation System (GLDAS), TerraClimate, and Gravity Recovery and Climate Experiment (GRACE), to assess the resiliency, reliability, vulnerability, and sustainability of river basin water management (Koudahe *et al.* 2017; Bherea & Reddy 2022; Salehie *et al.* 2022; Sharma *et al.* 2022). Climate change, in particular, has implications for how water resources are stored and managed. These problems are solved by implementing a CRA system, but changes in the weather patterns resulting from climate change can raise questions about its operations. Despite the increasing number of studies focused on improving the resilience of the agriculture sector, many questions still need to be answered regarding the effects of climate change on this sector. Moreover, understanding the temporal and spatial distribution of rainfall is also important in assessing the risks associated with various hydrological change events (Yang *et al.* 2020a, 2020b).

The lack of reliable climate data in various regions globally has hindered the development and implementation of climate simulation models and statistical analyses related to water resources, hydrology, and ecology. Thus, our research aims to provide insights into CRA system and water security goals over a 90-year period, encompassing both historical (1958–2020) and future (2021–2050) periods. Therefore, this study enquiring the various hydrometeorological conditioning factors and effects of climate change on current and future performance for the suitable CRA system. Climate uncertainty provides an opportunity to develop the CRA system under this framework. This type of initiatives can be applied to small- and medium-sized enterprises to enhance entrepreneurship and livelihood strategies for owners, as well as cultivate the attitudinal traits of successful proprietors. The United Nations is implementing the 2030 framework, consisting of 17 Sustainable SDGs, which serve as an urgent call to action for all countries worldwide. This approach represents a novel contribution to the field of Eastern Indian river basin management. What sets this research apart is its ability to provide precise and comprehensive methods for identifying climate-resilient groundwater management strategies. The study's primary focus is the development of a reliable Climate Resilience Assessment approach, specifically tailored to address the challenges posed by climate change in real-world

scenarios. The study aims to identify groundwater vulnerability zones, which will play a crucial role in alleviating water stress and preserving the hydrological ecosystem services and functions of the basin. Additionally, it will enhance the effectiveness of CRA management strategies in the region. This approach apart is its practicality – it not only advances theoretical understanding but also offers tangible solutions. Furthermore, it underscores ways to mitigate groundwater vulnerability, providing valuable insights for local practitioners. There have been limited studies on the changes in the hydrometeorological patterns in Ajay river basins. These studies also filing that gap to building the CRA system that influence these changes. In addition, few research on assessing the CRA system, only applied precipitation data and conventional statistical techniques, not apply the multisensor datasets for areas lacking the measured through the novel machine learning (ML) techniques. The study's findings were able to quickly do real-time assessment of direct impact of climate uncertainty on the vulnerability of agricultural productivity within the region. The novelty of this research, as well as the research gap filing it addresses, make significant contributions to the fields of groundwater conservation and climate change management. Various space-based multisensory datasets namely: TerraClimate, CMIP6, GLDAS, and GRACE, are employed for the measuring of water sustainability conditions in the Ajay River Basin region. In addition, this study envisions quantifying groundwater storage (GWS) resilience to analyze the future climate change resilience and its impact on achieving the SDGs at a river basin scale. The outcomes of this research will aid in identifying water stress zones and the necessary adaptation strategies required in any river basin.

2. MATERIALS AND METHODS

2.1. Study area

The Ajay River Basin lies in the eastern region of India and comprises between 23°20′–24°30′ North latitude and 86°15′–88°10′ East longitudes (Figure 1). The basin area covers around 6,081.49 km^2, with an elevation range of 3–707 m above means sea level. Originating from the Chhotanagpur plateau in the Santhal Pargana District of Jharkhand, the Ajay River and its associated basin extend across Dumka, Giridhi, and Deoghar in Jharkhand, as well as Jamui and Munger districts in Bihar, and Birbhum and Burdwan districts in West Bengal. The course of a river passes through different lithology, including the mega-physiographic regions of the Bengal basin and the Chhotanagpur massif. The upper portion of the course of a river flows through a unclassified gneissic structure. The middle reaches pass through Gondwana complex and the lower part of the course is also underlain by sequences of sediment with quaternary structure (Bhattacharya 1972). The area under study has undulating topography with gentle slopes toward the southeast and east, with varying elevations. The large portion of pedocal soil that extends over the Ajay River Basin. The Katwa Surface is characterized by an alluvial soil that has already

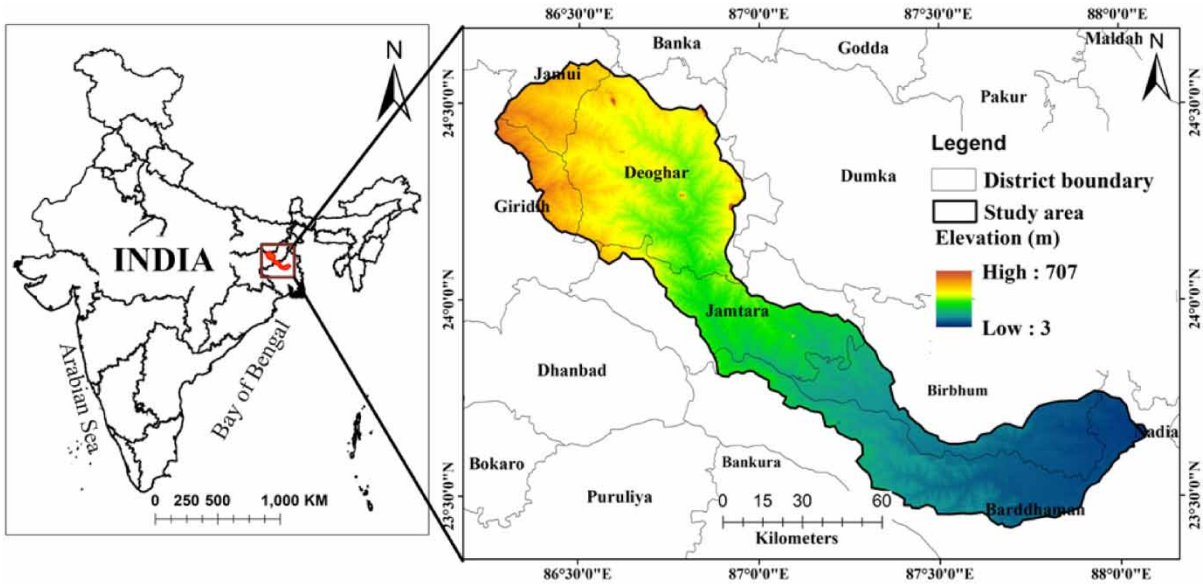

Figure 1 | Study area map.

undergone active soil formation in the lower part of the basin (Geological Survey of India 1985). The extreme variability of the rainfall during the monsoon season significantly affects the hydrological conditions of the Ajay River Basin (Niyogi 1988). This river basin experiences monsoonal rainfall around a mean of 1,278–1,322 mm annually (India Meteorological Department (IMD) 2018). The summer and winter temperature varies from 25 to 37 °C and 10 to 24 °C, respectively. The Ajay River flows through recent alluvium and is subjected to a moderate to high discharge. Flash floods in the Ajay River occur frequently. Due to the availability of irrigation facilities, fertile alluvial soil, and ample soil moisture, this region is primarily engaged in highly productive agricultural practices, including the cultivation of crops such as rice, potatoes, oilseeds, and various horticultural crops (Banerjee *et al.* 2021). The majority of the land in the basin is dedicated to cropland, covering an area of 3,499.14 km^2 of the total basin area (ST 1, URL: European Space Agency (ESA) https://esa-worldcover.org/en). The concentration of forest land is highest in the right bank around 13.17%, as opposed to the left bank.

2.2. Data

The historical monthly climatic data collected during the study were analyzed through the TerraClimate platform (1958–2020) with a spatial resolution of 4,638.3 m. The TerraClimate dataset has been previously evaluated over surrounding regions and countries and had very good accuracy (Filgueiras *et al.* 2022; Araghi *et al.* 2023). Terrestrial water storage (TWS) data were acquired from the NASAs GRACE (2002–2021) mission with a spatial resolution of 111,320 m. The GLDAS (2003–2021) datasets were analyzed in the Google Earth Engine (GEE) cloud API. The spatial resolution of the GLDAS v2.2 datasets were 27,830 m. The historical and future climatic condition was assessed under 245, and SSP585 scenarios through CMIP6 GCMs (i.e. MIROC6 and EC-Earth3) (2021–2050) with a spatial resolution of $0.25° \times 0.25°$. Additionally, Our analysis encompasses a total of 90 years of model outputs, including temperature and precipitation, spanning both the historical period (1958–2020) and the future period (2021–2050) for climate change analysis.

2.2.1. Groundwater level data

In total, 22 district-wise pre-monsoon groundwater level (mbgl) data (2018–2019) were collected from the Central Ground Water Board (CGWB, India) (URL: http://cgwb.gov.in/GW-data-access.html). Inverse distance weighting (IDW) spatial interpolation techniques were used for the spatial distribution of the groundwater level inventory mapping within the river basin. Furthermore, this map was used for validation and sensitivity analysis in our study of CRA and water sustainability in this region.

2.3. Methodology

In the current study, different climatic variables such as maximum temperature (T_{max}), minimum temperature (T_{min}), and precipitation, as well as the hydrological variables such as actual evapotranspiration (AET), potential evapotranspiration (PET), runoff (Q), vapor pressure deficit (VPD), and climate water deficit (DEF), were analyzed for a period of 62 years (1958–2020) to determine the annual climatological and hydrological characteristics of the study area. The GRACE solutions were employed to estimate equivalent water thickness (EWT) provided by the Center for Space Research (CSR) and the Jet Propulsion Laboratory (JPL), at the University of Texas, Austin covering the period from 2012 to 2021. Similarly, the water balance system was estimated using TWS and GWS data from the GLDAS v2.2 model for the years 2003–2021 (Bherea & Reddy 2022; Equations (1) and (2)):

$$\Delta TWS = \Delta GW + \Delta SM + \Delta SWE + \Delta SW \quad (1)$$

where ΔGW is the groundwater, ΔSM is the soil moisture, ΔSWE is snow water equivalent, and ΔSW is surface water.

$$\Delta GWS = \Delta TWS - \Delta RSM - \Delta SWE - \Delta CI \quad (2)$$

where ΔTWS is terrestrial water storage, ΔRSM is the root zone soil moisture, ΔSWE is snow water equivalent, and ΔCI is canopy interception.

The IDW interpolation method was used to develop the spatial distribution of climatic and water sustainability mapped from the global TerraClimate, GRACE, and GLDAS datasets in the ArcGIS environment. The details workflow of the methodological framework is represented in Figure 2.

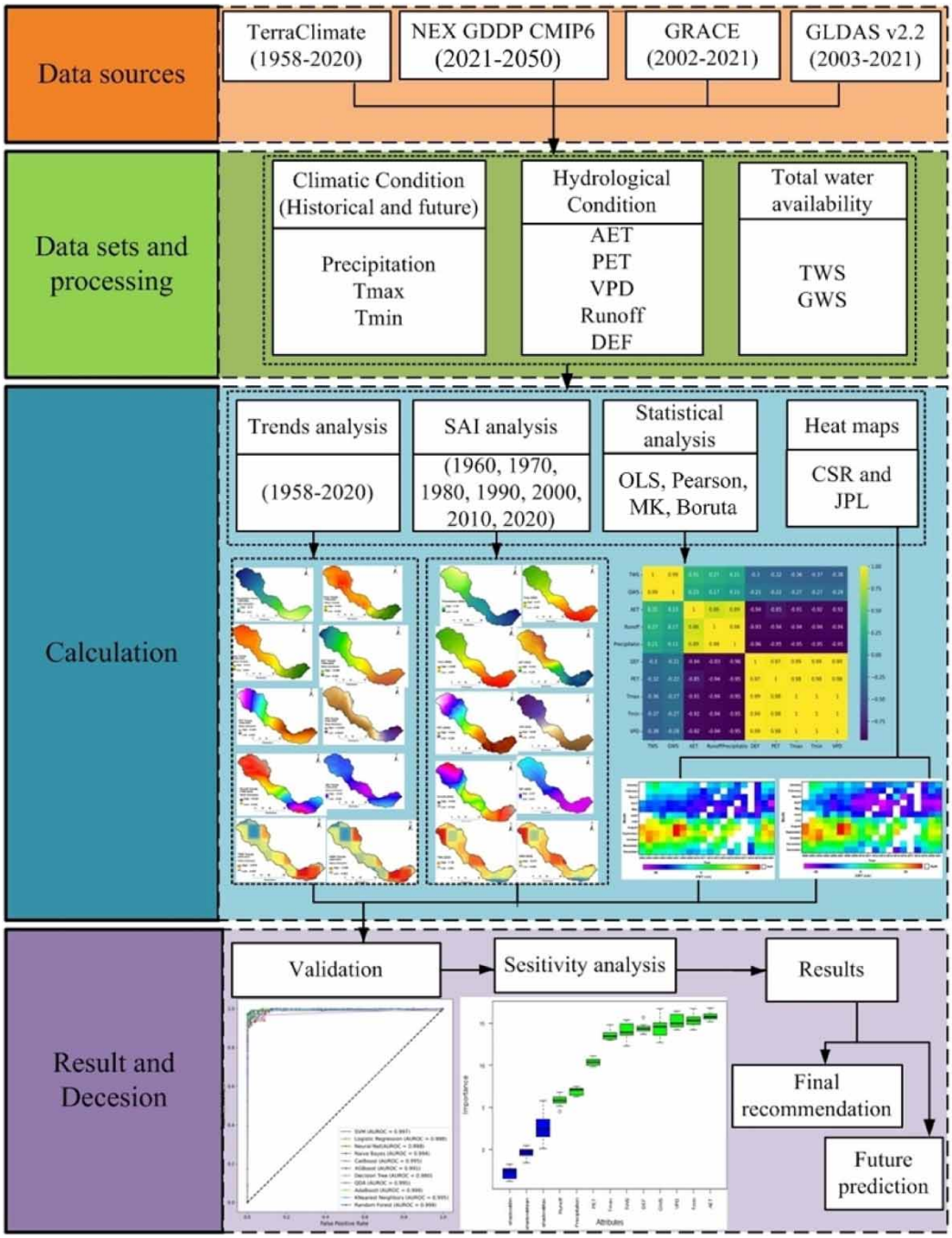

Figure 2 | Workflow of details methodology for water sustainability.

2.3.1. Statistical trend analysis and anomaly index

The linear regression derived (*ee.Reducer.linear Fit)* estimator was employed to show the long-term trends (1958–2020) of all annual climatological and hydrological variables changes. Similarly, the SAI was used to identify the significance trends of the hydrometeorological parameters. Furthermore, statistical significance analysis was computed using the ordinary least square (OLS) regression method, which revealed a statistically significant relationship exceeding 99% ($p < 0.001$) between GWL and hydrometeorological predictors. Metrics such as R^2, Prob $> \chi^2$, and F statistic were used to assess the effectiveness of OLS assumptions among the predictors, demonstrating an adjustment level exceeding 99% significance (Hidalgo-García &

Arco-Díaz 2022). The calculation for linear regression, SAI, and OLS were computed using the following equations (Bilginola *et al.* 2015; Koudahe *et al.* 2017; Equations (3)–(5)):

$$Y_i = \beta_0 + \beta_1 x_i + \varepsilon_i \tag{3}$$

where Y_i is the dependent variable, β_0 is population Y-intercept, β_1 is slope coefficient, $\boldsymbol{x_i}$ is the independent variable, and ε_i is a random error:

$$\text{SAI} = \frac{(x - \mu)}{\sigma} \tag{4}$$

where x is the yearly average, μ is the long-term average, and σ is the standard deviation:

$$\hat{\beta} = (X^\top X)^{-1} X^\top y \tag{5}$$

where $\hat{\beta}$ is the OLS estimator, X represents the matrix regression of X, $\top$ is a matrix transpose, and y is a trajectory of the value of the response.

Climatological and hydrological trend analysis and anomaly indices are interpreted as follows: negative values indicate a declining trend, while positive values suggest an increasing trend. SAI was analyzed for the TerraClimate parameters with 10-year intervals (i.e., 1960, 1970, 1980, 1990, 2000, 2010, and 2020), while GLDAS analysis covered the years 2005, 2010, 2015, and 2020. Monthly GRACE solution data (CSR and JPL) were averaged over the study area to provide the anomaly of ETW in centimeters during the period from 2012 to 2021. GRACE-based ETW heat maps were used to visualize the regional water balance patterns. Additionally, the Pearson correlation coefficient was employed to quantify the relationships among all hydrometeorological variables. These visualizations and assessments were generated using the *Matplotlib* library in Anaconda Python 3 software.

The study also showed the intercomparison of the historical climatic trends (1958–2020) through the Mann–Kendall (MK) test of the entire basin region (Dhar *et al.* 2014). The following equations are applied for the calculating the MK test (Mann 1945; Kendall 1975) (Equation (6)):

$$S = \sum_{i=1}^{n-1} \sum_{j=i+1}^{n} \text{sgn}(d_j - d_i) \tag{6}$$

where n denotes the number of sample location, di and dj are the data scores in time series i and j ($j > i$), respectively, and $\text{sgn}(d_j - d_i)$ represents the sign function. The standard normal test statistic Z_S is calculated as (Equation (7)):

$$Z_S = \begin{cases} \dfrac{S-1}{\sqrt{\text{Var}(S)}}, & \text{if } S > 0 \\ 0, & \text{if } S = 0 \\ \dfrac{S+1}{\sqrt{\text{Var}(S)}}, & \text{if } S < 0 \end{cases} \tag{7}$$

where the variance is formulated using (Equation (8)):

$$\text{Var}(S) = \frac{n(n-1)(2n+5) - \sum_{i=1}^{m} t_i(t_i-1)(2t_i+5)}{18} \tag{8}$$

where m represent the number of tied class and t_i is the number of ties of extent i. A Positive Z_S specified an increasing trend, while a negative Z_S reveals a decreasing trend.

2.3.2. Validation and sensitivity analysis

The current study employed ten ML classification models, i.e. random forest (RF), support vector machine (SVM), Naïve Bayes (NB), logistic regression (LR), neural network (NN), CatBoost (CAB), extreme gradient boosting (XGB), AdaBoost (ADB), decision tree (DT), quadratic discriminant analysis (QDA), and k-nearest neighbors (KNN), for the final GWS validation analysis.

RF

RF model used for both classification and regression problem. RF combines the training of a regression tree with the boosting technique to produce a large number of efficient tree models (Breiman 2001). Each of the training trees is analyzed using a randomly chosen set of variables by the voting classifier. The last predictor of the model is calculated by considering the results of the other trained trees.

SVM

The non-linear problems are mapped into a higher dimensional space in SVM, which makes them easier to solve with the help of the kernel functions (i.e. linear, radial, polynomial, and sigmoid) (Cortes & Vapnik, 1995). The selection of the appropriate kernel function is very important in order to develop prediction models that are derived from this framework.

NB

The NB classifier is a part of the group of posterior probabilistic classification systems that are based on Bayes' Theory (Mushtaq & Mellouk 2017). It assumes that all the variables are independent and can be studied separately. This allows the system to perform faster and simpler analysis through the 'parent node' and 'child' node system.

LR

The LR model can also be utilized to analyze the link between a given variable and several independent ones (Kim *et al.* 2019). Due to the nature of a binary dependent variable, it can lead to various issues, like predicted values and errors in which the ranges from 0 to 1. LR is a better alternative to performing a comprehensive analysis of such variable.

NN

Hidden layer-based NN used to take complex decision. The NN topology might be developed through a trial-and-error approach to address the hidden layer's number. The NN framework assigns varying weights to the inputs in order to perform prediction calculations (Kumar *et al.* 2002). An error minimization method is then used to finetune the predictions in subsequent iterations.

CAB

The CatBoost algorithm was utilized to perform with gradient-enhanced DT algorithm (Prokhorenkova *et al.* 2018). It will extracted variables as categorical type. The collected data is then randomly generated and presented with various random sequence of feature combinations method.

XGB

One of the most popular implementations of the gradient boosting machine (GBM) algorithm is Xgboost (Chen & Guestrin 2016). It is regarded as a superior performer in supervised learning. It can be applied for both classification and regression problems.

ADB

ADB model was implemented with the boosted decision trees that are dealing with binary classification issues (Freund & Schapire 1995). It is perfect utilized with weak learners for the classification problems.

DT

The supervised MLas DT method is commonly used to split a set of factors into multiple decision trees. Generally, the DT prediction tree structure used for classification regression and classification problem (Kadavi *et al.* 2019). The three nodes that make up DT are the root node, internal node, and leaf node. The outcome is then displayed as root node, internal node and leaf nodes in the dataset. The DT algorithm is utilized to divide the data into smaller classes.

QDA

The QDA is a flexible and classical classification method that allows groups to be distinguished according to covariance matrix and mean vectors (Qin 2018). In the classical QDA framework, the sample covariance matrix is high-dimensional, its singularity can occur.

K-nearest neighbor (KNN)

The kNN algorithm is widely used in supervised learning. It can predict new data points with accuracy of approximating their proximity (Zhang & Zhou 2007). The assigned values for these predictions are based on the training set's points.

The KNN algorithm run with the following steps, namely first estimated the nearest neighbors of the k value, next classify datapoints through the Euclidean distance measure and then sort the training sample and finally majority of the nearest neighbors decided the final prediction.

All ML models were trained and tested using both calibration (70%) and validation (30%) datasets. The groundwater level (district level) was the target variable, while all the hydrometeorological parameters (SAI of 2020) were considered independent variables. The performance of each ML model was assessed using robust evaluation statistical metrics, including accuracy, precision, recall, F1 score, and the area under the receiver operating characteristics curve (AUROC) (Singha & Swain 2022; Equations (9)–(13)). The ML-based validation analysis was carried out by the *sklearn* library in python3:

$$\text{Accuracy} = \frac{\text{TP} + \text{TN}}{\text{TP} + \text{FP} + \text{TN} + \text{FN}} \tag{9}$$

$$\text{Precision} = \frac{\text{TP}}{\text{TP} + \text{FP}} \tag{10}$$

$$\text{Recall} = \frac{\text{TP}}{\text{TP} + \text{FN}} \tag{11}$$

$$\text{F1Score} = 2 * \frac{\text{precision} * \text{recall}}{\text{precision} + \text{recall}} \tag{12}$$

$$\text{AUROC} = \frac{\sum \text{TP} + \sum \text{TN}}{\text{TP} + \text{TN} + \text{FP} + \text{FN}} \tag{13}$$

where TP is True Positive; TN is True Negative; FP is False Positive; FN is False Negative

Boruta feature selection techniques were employed to prioritize the sensitivity parameter of TWS sustainability. This analysis was carried out on the relevant dataset using the RF classifier with the BorutaPy library in Anaconda Python 3. This new approach allows us to identify the most important variables in the CRA system (FAO, 2020).

3. RESULTS

3.1. Trend analysis of historical climatic and hydrological parameters

The present study examines the long-term trend maps (slope of the linear regression) for precipitation, T_{max}, T_{min}, AET, PET, VPD, Runoff, DEF, TWS, and GWS variables over the study domain. In Figure 3, it is evident that the southern region exhibits a more concentrated negative trend in precipitation (approximately −0.04 mm/year), while the northern region shows a positive trend (around 0.10 mm/year) . The gradient of the T_{max} and T_{min} trend varies from north (maximum) to south (minimum). The slope of the AET trends represent from south (positive ~ 0.080 mm/year) to north (negative ~ −0.006 mm/year). The rate of PET trends ranges from −0.033 to 0.064 mm/year, with most of the area experiencing a high VPD trend (around 0.00008 kPa/year), except for the southern part (around −0.00027 kPa/year). Turnoff trends are highest in the northern part (around 0.027 mm/year), and the distribution of high and low DEF trend values varies from 0.007 mm to −0.039 mm across the study area. Positive DEF trends are observed in the central part, while negative trends are concentrated in the upper and lower regions. GLDAS v2.2 derived TWS and GWS trend values vary from −8.607 to −5.976 mm/year and −6.883 to −4.886 mm/year, respectively. Conversely, the moderate to low TWS trends are found in the northern region. The spatial direction of the GWS trends varies from the lower (high) to the upper part (low) of the region.

3.2. Trend analysis of future climatic conditions

Spatial pattern maps of the future precipitation, T_{max}, and T_{min} trends (SLR) were generated using the CMIP6 SSP2-4.5, SSP5-8.5 and historical dataset (2021–2050) for the Ajay River Basin. All the scenarios are estimated through the two different type of general circulation models (GCMs) models i.e. MIROC6 and EC-Earth3 ((Tatebe *et al.* 2019; Sahoo & Govind 2023).

3.2.1. MIROC6 general circulation model (GCM)

In Figure 4(c), the future precipitation pattern shows a negative trend in the lower part of the basin (around −0.000042 mm/year) and a positive change in the upper part (around 0.000027 mm/year) through the SSP2-4.5 scenario. This indicates that the lower region will likely have lower infiltration rates, potentially providing adequate abstraction for water storage. Conversely, the upper part is expected to experience higher runoff and flash flood hazard events in the upcoming decades. Similar

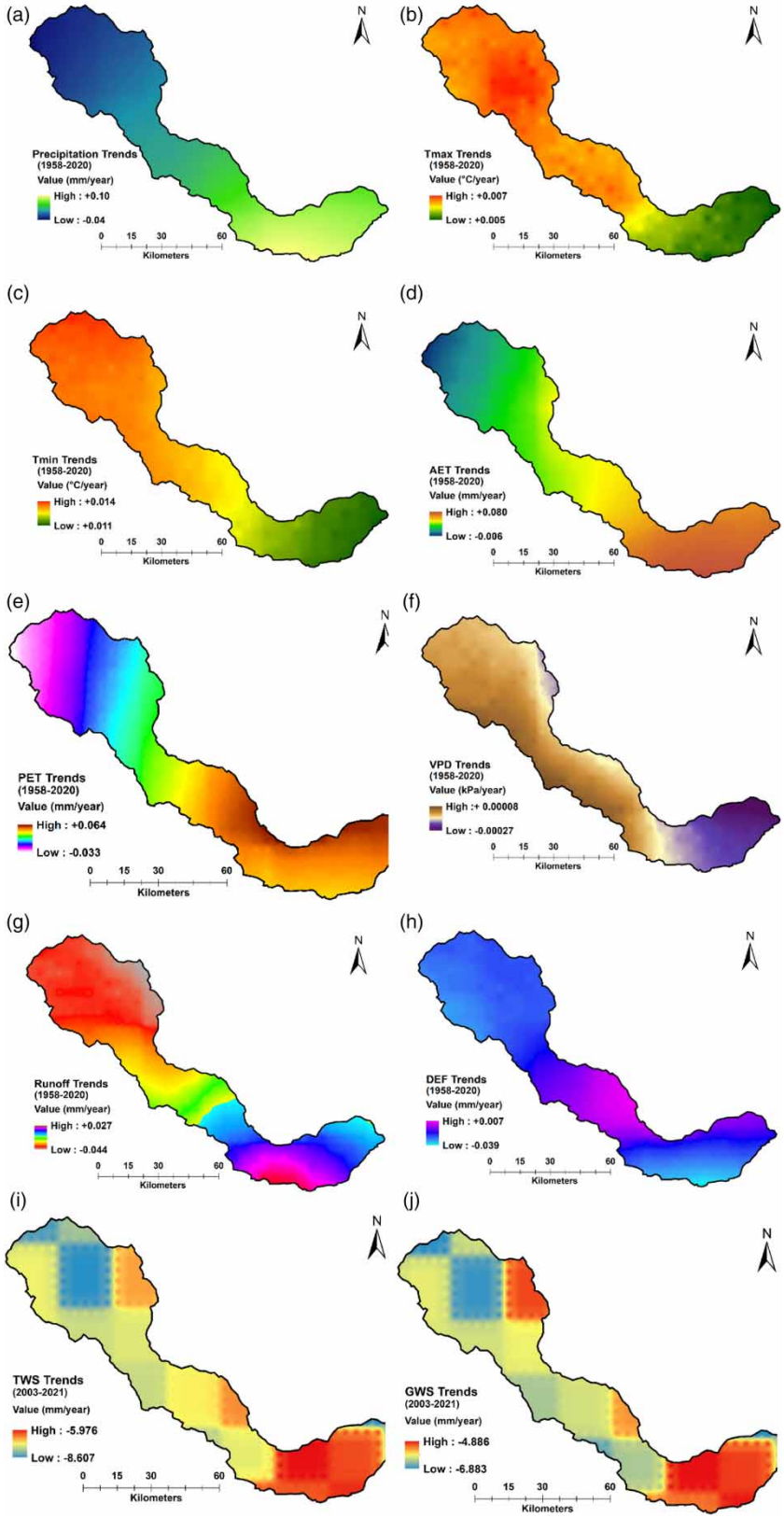

Figure 3 | Trend analysis of historical climatic and hydrological parameters: (a) precipitation, (b) T_{max}, (c) T_{min}, (d) AET, (e) PET,(f) VPD, (g) runoff, and (h) DEF, (i) TWS, and (j) GWS in the study area.

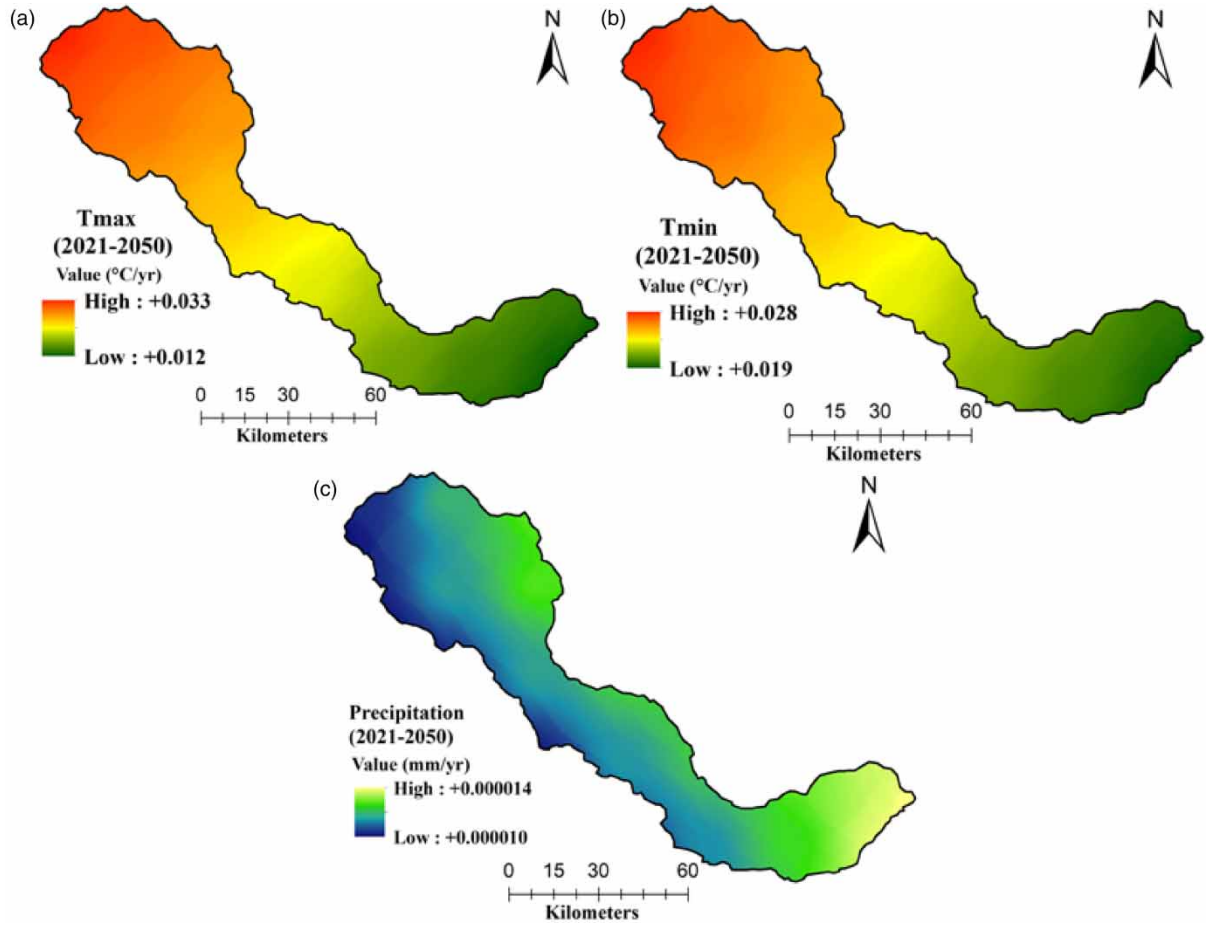

Figure 4 | Spatial pattern maps of the future: (a) T_{max}, (b) T_{min}, and (c) Precipitation, for the MIROC6 CMIP6 model (SSP2-4.5) in the study area (2021–2050).

inconsistencies are observed in the variability trends of average annual T_{max} and T_{min} across the study area. Variability in T_{max} and T_{min} is notably higher in the northern part (0.035–0.037 °C/year) compared to the southern part (0.030–0.033 °C/year) (Figure 4(a) and 4(b)). These findings suggest that the southern part is more likely to experience high AET and PET, increasing the likelihood of water stress conditions and a higher probability of drought hazards during 2021–2050 in the lower Ajay River Basin.

Based on the SSP5-8.5 scenario in MIROC6 model, the linear trends of T_{min} and T_{max} value varies between 0.013 to 0.034 °C/year and –0.021 to 0.012 °C/year. The recorded trend of the annual precipitation ranges form 0.000026 mm/year in the northern part to 0.000031 mm/year in the southeast (Figure 5(c)).

The historical trend (1958–2020) of T_{max} and T_{min} ranges from −0.021 to 0.007 °C/year (Figure 6(a) and 6(b)). Similarly, the historical trend of MIROC6 model showed the negative trend of precipitation in the southern part of the region around −0.0000026 mm/year) and a positive change in the northern part around 0.00000063 mm/year).

3.2.2. EC-Earth3 general circulation model (GCM)

According to the EC-Earth3 model (SSP2-4.5) (Sahoo & Govind 2023), the trend of T_{max} and T_{min} ranges form 0.003 °C/year in the north to 0.025 °C/year in south (Figure 7(a) and 7(b)). Therefore, the trend of the annual precipitation ranges recorded form −0.0000015 mm/year in the south of the basin to 0.0000074 mm/year in the north (Figure 7(c)).

Figure 8(a) and 8(b) showed similar trend of T_{max} and T_{min} variable in the study area. Maximum and minimum T_{max} and T_{min} found in north and south of the basin. Figure 8(c) showed the positive precipitation trend ranges from 0.0000016 to 0.0000041 mm/year with the EC-Earth3 SSP5-8.5.

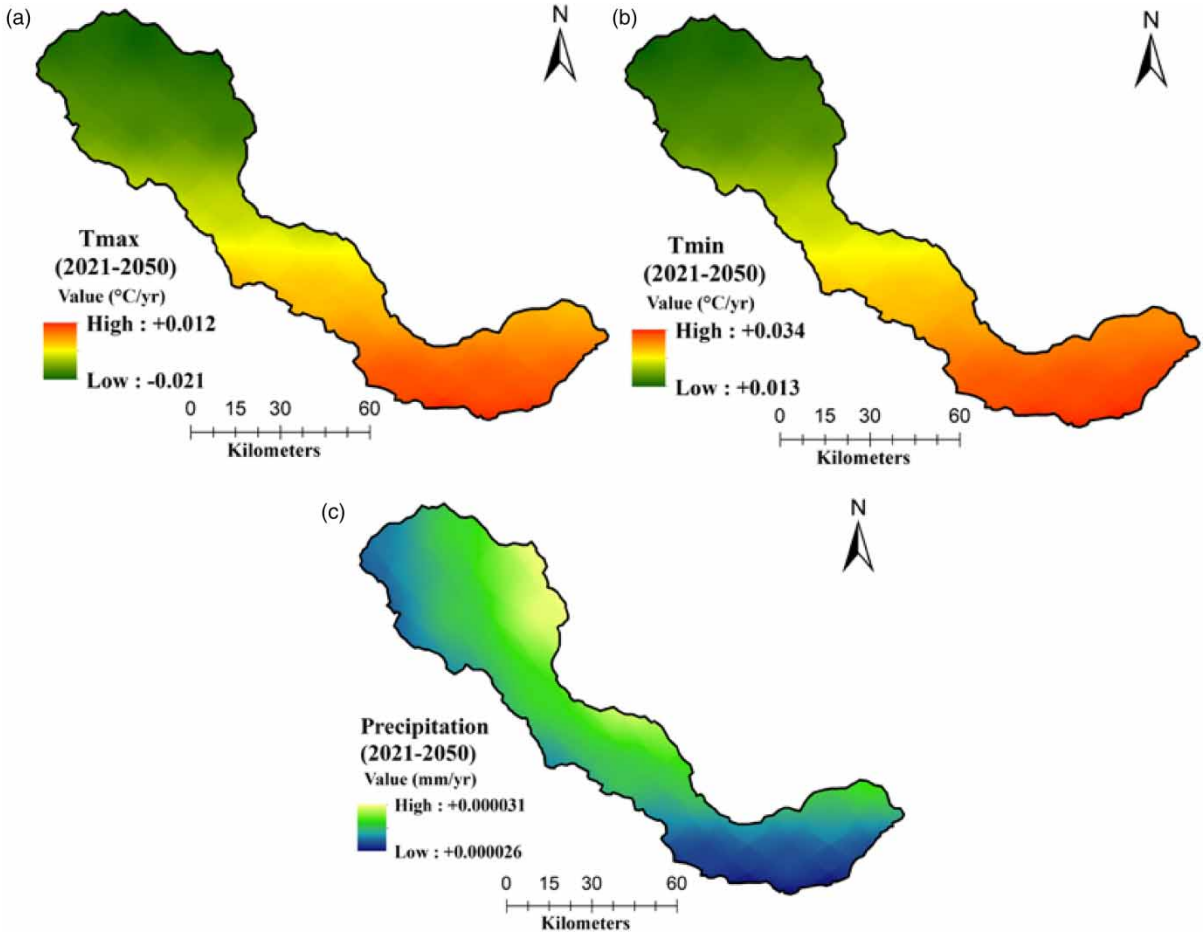

Figure 5 | Spatial pattern maps of the future: (a) T_{max}, (b) T_{min}, and (c) Precipitation, for the MIROC6 CMIP6 model (SSP5-8.5) in the study area (2021–2050).

The historical EC-Earth3 model calculated the T_{max} and T_{min} is notably higher in the northern part (-0.013 ± 0.010 °C/year) compared to the southern part (0.016–0.018 °C/year) (Figure 9(a) and 9(b)). Similarly the spatial trend of the precipitation ranges form 0.0000067 mm/year in the low northwest to 0.0000097 mm/year in southeast in the study area.

3.3. SAI analysis of climatic and hydrological parameters

Supplementary material, Figures S1–S10 show the spatial distribution of long-term SAI maps for the Ajay River Basin. The precipitation showed a similar pattern to SAI: high in the southern part and low in the northern part except for the years 1980, 2010, and 2020. Negative SAIs were observed for the years 1980, 2000, and 2010, while positive SAIs were noted for 1990 and 2020 (Supplementary material, Figure S1). The spatial pattern of the T_{max} is very low in 1990 (-0.105 to -0.087) compared to other years (Supplementary material, Figure S2(d)). The SAI of T_{min} over the study domain specified that southern part has higher T_{min} value (i.e., 1960, 1970, 1980, 1990 and 2020) compared to other years (Supplementary material, Figure S3). Supplementary material, Figure S4 shows the positive SAI of AET for the years, e.g., 1990, 2000, and 2020, while that only negative SAI recorded in 1960. SAI of PET displayed a relatively consistent pattern across the region, with maximum PET identified over the southern part in 1980, 1990, 2010, and 2020, and minimum PET found in the northern part in 1960 and 1970 (Supplementary material, Figure S5). Negative runoff was observed in 1980, 2000, and 2010, while positive values were recorded for 1970, 1990, and 2020 (See Figure 6). The positive SAI of DEF value was observed in 1960 and 2010, while more negative values were found during 1990, 2000, and 2020, respectively. Negative DEF (>0.005) was recorded during 1970–1980 in the northern part of the basin, while positive DEF values (below -0.02) were seen in the southern part. This indicates temporal and spatial variation in water suitability (Supplementary material, Figure S7).

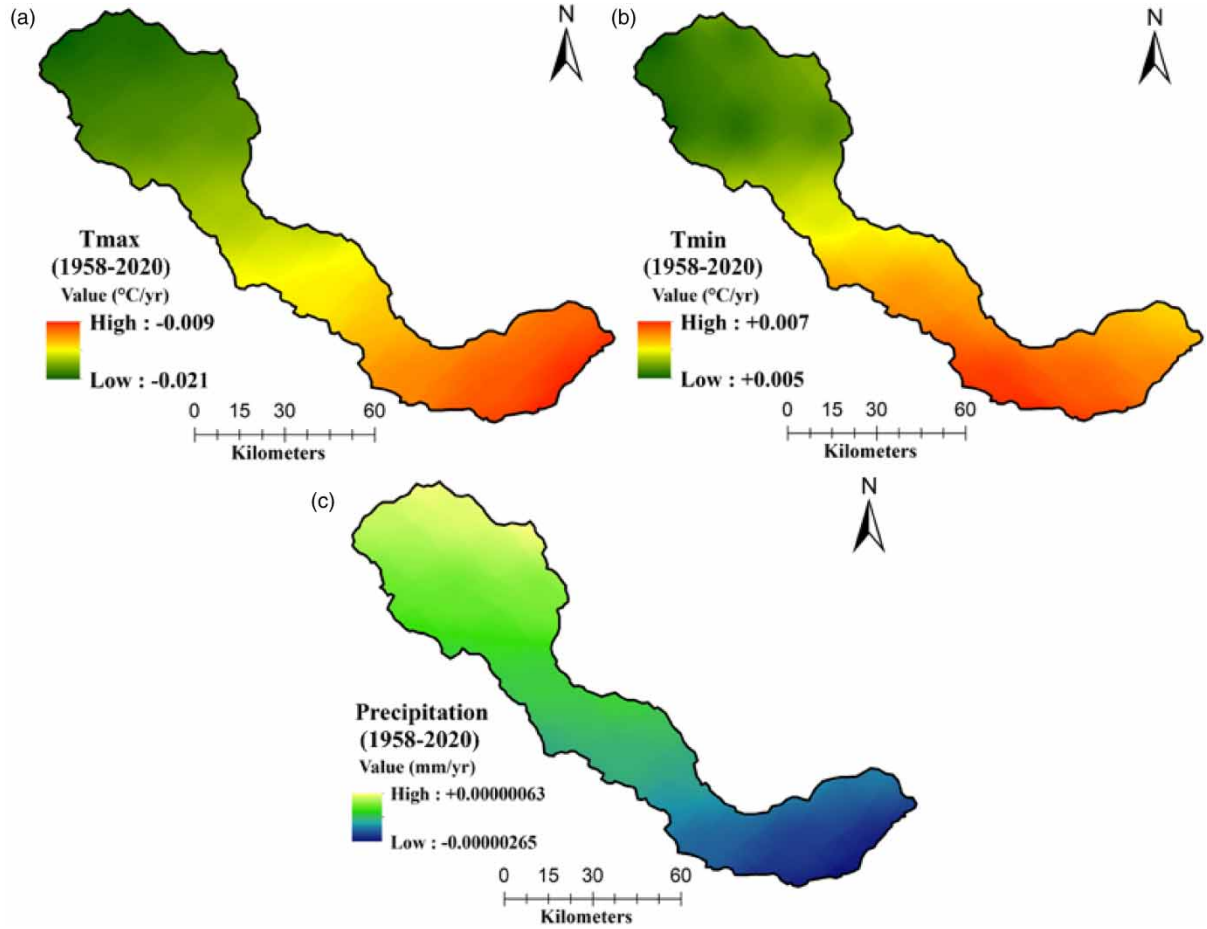

Figure 6 | Spatial pattern maps of the future: (a) T_{max}, (b) T_{min}, and (c) Precipitation, for the MIROC6 CMIP6 model (historical) in the study area (1958–2020).

In Supplementary material, Figure S8, the majority of the basin had SAI values greater than 0.005 for VPD in 1960 and 2010, with mostly negative SAIs occurring from 1970 to 1990. In 2020, the SAI of VPD was highest in the lower part and lowest in the upper part of the basin. Supplementary material, Figure S9(a)–(f) display the SAI of GWS, with maximum values (>0.3) observed over the northern part during 2005, 2015, and 2020. Completely negative SAI of GWS was seen only in 2010 (Supplementary material, Figure S9(b)). Similarly, positive SAI of TWS was observed during 2005, with higher positive values, and during 2020, it had the highest positive value (around 1) in the southern part of the study domain (Supplementary material, Figure S10(d)). Based on SAI maps of GWS and TWS, the spatial pattern of water availability exhibited a declining trend from 2015 to 2020 in the southern part, except in 2015. In 2020, the earlier years showed very low precipitation, AET, runoff, TWS, and GWS values in the southern part, whereas T_{max}, T_{min}, PET, VPD, and DEF exhibited the opposite conditions (Supplementary material, Figure S11).

The annual precipitation, T_{max}, and T_{min} time series were analyzed using the MK trend test of the study area domain (1958–2020). It was used to identify potential trends in the data. Table 1 shows MK test statistic (S), calculated Z_S values, p value and tau conditions. Based on the S score, precipitation had 47, T_{max} had 229.01 and T_{min} had 713.05. According to the significant analysis ($p < 0.05$), all the three climatic parameters are significant. The results of trend agreement with the critical Z and tau values for the precipitation, T_{max} and T_{min} were recognized i.e. 2.216, −9.71, 4.22 and 0.013, −0.054, 0.365, respectively.

3.4. Temporal distribution of current water storage conditions

Supplementary material, Figure S12 represents the spatial-temporal variability of monthly EWT anomalies during 2002–2021 in the Ajay River Basin. The ETW values from both the CSR and JPL products varies form −37.97 to 38.30 cm. Temporal

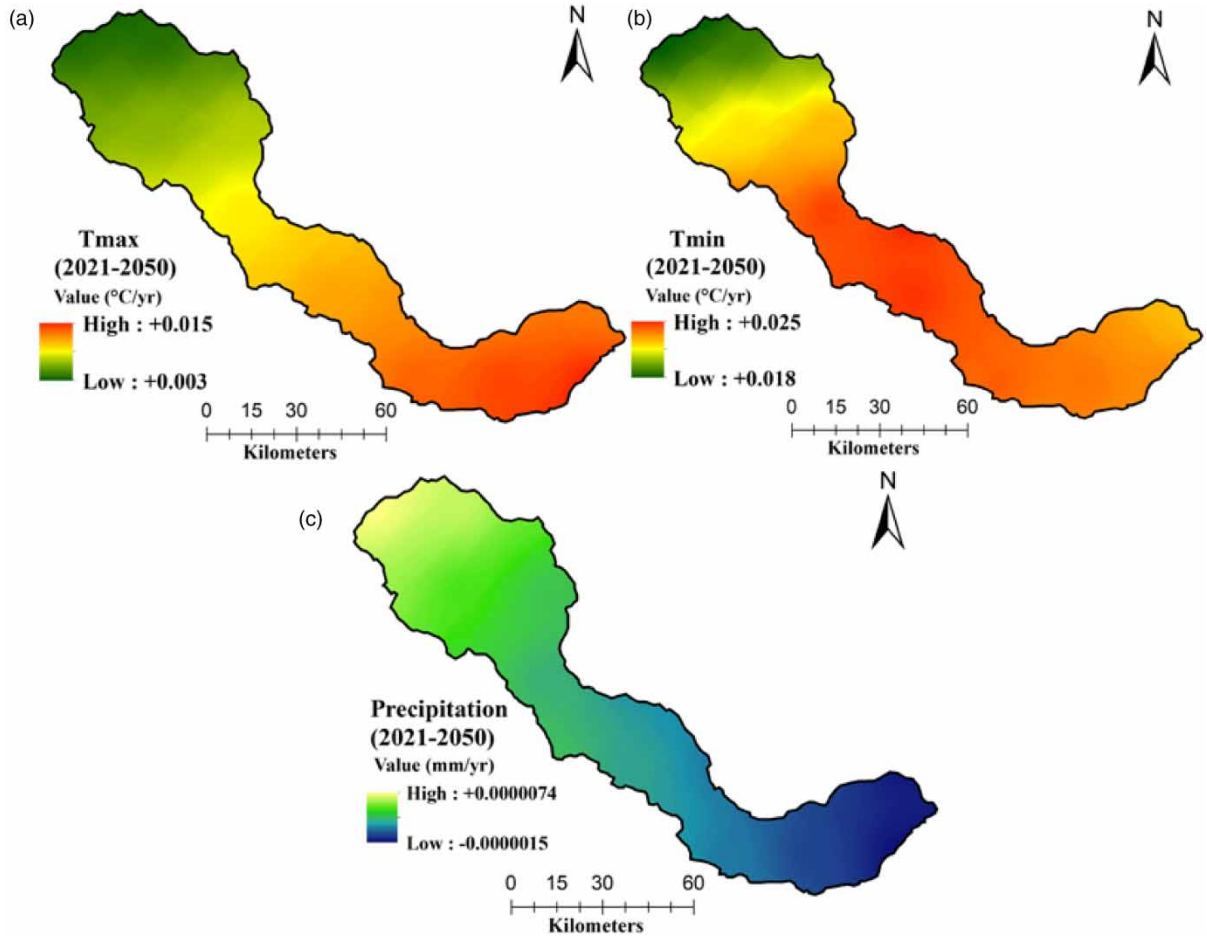

Figure 7 | Spatial pattern maps of the future: (a) T_{max}, (b) T_{min}, and (c) Precipitation, for the EC-Earth3 CMIP6 model (SSP2-4.5) in the study area (2021–2050).

variability in high EWT is evident in the early years during the pre-monsoon. It signifies a recurrent fluctuations in water resources in the study region. However, water consistency was higher in 2007 and 2008. EWT values were typically above the mean level (indicating positive changes) from July to November (post-monsoon) and below the mean level (indicating negative changes) from December to June (pre-monsoon) across the region. Both GRACE products (CSR and JPL solutions) exhibited regular variation in seasonal EWT variability. In recent years, the EWT trend had gradually declined. For example, it was generally above the mean level in post-monsoon, while lower than the mean level in pre-monsoon. he JPL-derived EWT showed a lower mean level from March to May (2006–2021), while the CSR-derived EWT showed this from April to May (2009–2021). These findings collectively suggest that water availability has increased in recent years in the region, although the EWT results from the two products were not entirely consistent for this region. Both GRACE products exhibited an increase in purple color in recent years, indicating a poor EWT. Based on the EWT heat maps, the historical years characterized high availability of water during 2002–2008, while recent years have shown a decreasing trend in EWT from 2009 to 2021, with concentrations in 2013 and 2021 (Figure 10).

3.5. Correlation of hydrometeorological parameters

The study further scrutinizes the association among different climatic and hydrological input parameters using the statistical Pearson correlation matrix, OLS, and Boruta feature importance technique. The GWS and TWS have a positive correlation with AET, runoff, and precipitation as well as an anticorrelation with the DEF, PET, T_{max}, T_{min}, and VPD parameters, respectively (Supplementary material, Figure S13). The correlation of AET is very strong with runoff and precipitation (above 0.85). Similarly, DEF showed strong positive correlations with the VPD (0.99), PET (0.97), T_{max} (0.99), and T_{min} (0.99) parameters,

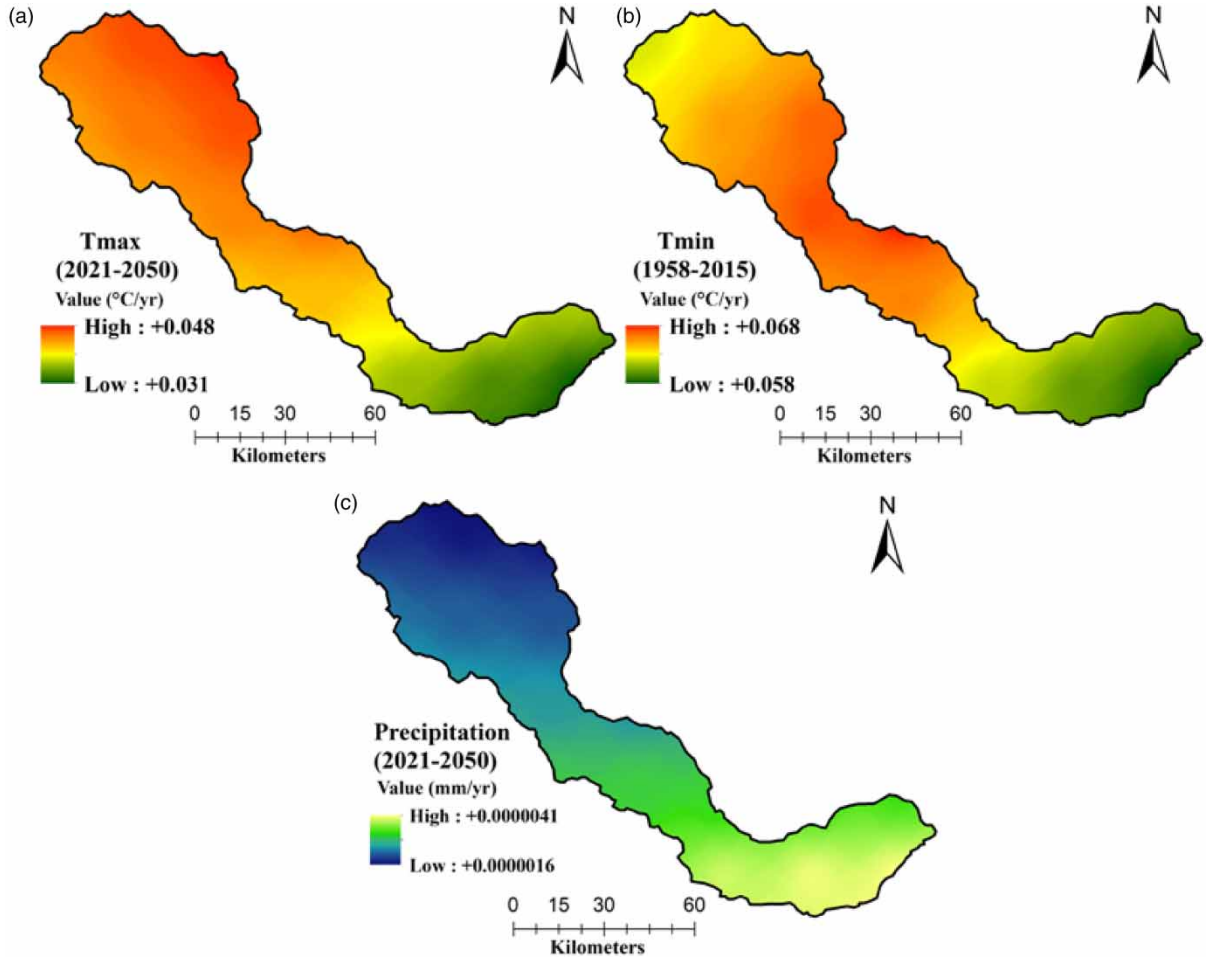

Figure 8 | Spatial pattern maps of the future: (a) T_{max}, (b) T_{min}, and (c) Precipitation, for the EC-Earth3 CMIP6 model (SSP5-8.5) in the study area (2021–2050).

Table 1 | Mann–Kendall trend test for the climatic data (1958–2020)

	z	*S*	*p*	tau
Precipitation	2.216	47	0.027	0.013
T_{max}	−9.714	229.01	0.000	−0.054
T_{min}	4.223	713.05	0.000	0.365

as well as an inverse relationship with AET (−0.94), runoff (−0.93) and precipitation (−0.96). Based on OLS evaluation, the GWS, runoff, precipitation, PET, DEF, and AET are statistically significant over >99% ($p < 0.001$), while TWS and T_{min} are statistically significant over < 95% ($p < 0.05$) (Table 2). The coefficient range value varies from −3.91 to 3.56 while the values of R^2 (0.93), F statistic (1311), and Durbin–Watson (1.396), Prob > χ^2 (0.00) indicated a good concordance among the input parameters with satisfactory results.

3.6. Validation and sensitivity analysis

This study used *in situ* district wells of groundwater level data for validation purposes. Figure 11 represents the average depth to groundwater level for the period of pre-monsoon (2018–2019). The average depth of groundwater level was around 10.91 mbgl. It was observed that the groundwater level of the study area varies between 6.631 and 15.78 mbgl. According to the

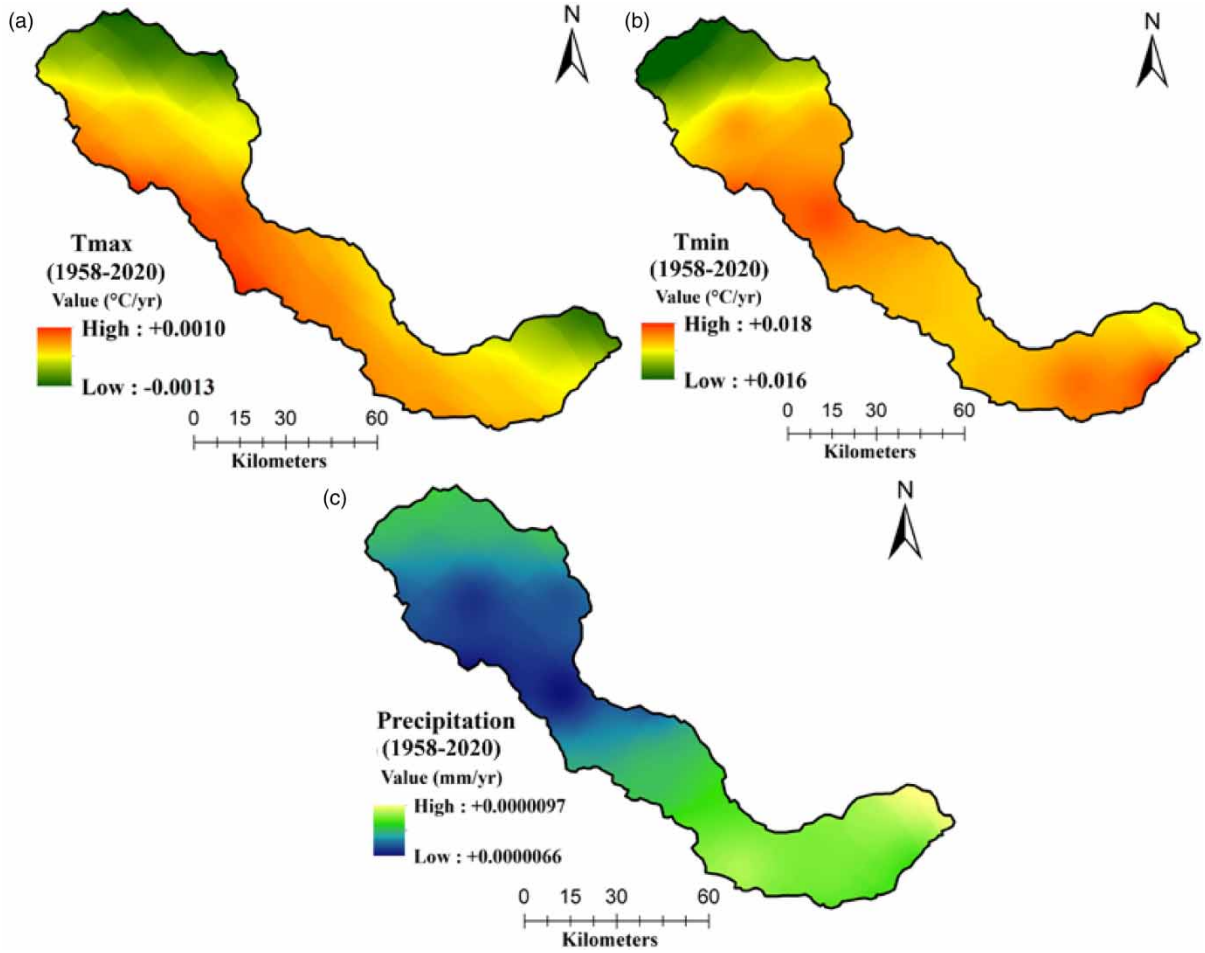

Figure 9 | Spatial pattern maps of the future: (a) T_{max}, (b) T_{min}, and (c) Precipitation, for the EC-Earth3 CMIP6 model (historical) in the study area (1958–2020).

groundwater level map, the lower part of the basin had a high fluctuation rate of groundwater level from 12.70 to 15.78 mbgl, while the upper part had a moderate to low fluctuation rate groundwater level from 6.631 to 9.670 mbgl. In this study, the groundwater level data was assigned with the threshold value of 10.91 mbgl (mean value) which specified the probability range in the binary alignment ('0'~ moderate to a very low level, >10.91 mbgl, and '1'~ moderate to a very high level, <10.91 mbgl). In total 960 randomly selected field locations were used for model validation.

The optimal scores obtained after the validation of the ten ML models are presented in Table 3. The performance of each ML model was evaluated using various statistical metrics (Table 2). Based on the AUROC results, the ADB and RF models reached the best score (0.999), followed by the LR (0.998), NN (0.998), SVM (0.997), CAB (0.995), QDA (0.995), KNN (0.995), NB (0.994), XGB (0.991), and DT (0.980) models, respectively (Supplementary material, Figure S14(a)). ADB and XGB model are the best performers with 99% train and test accuracy compared to other ML models. The combined precision and recall values were higher than 95% for the XGB, ADB, CAB, RF, and KNN models. Based on the F1 score (around 98%), the XGB, ADB, and KNN models were the top three performers.

According to the Boruta technique, all the hydrometeorological factors were confirmed as the most prioritized decision for the water storage analysis (Table 4). The Boruta feature importance, based on RF, was employed for parameter sensitivity analysis with 99% accuracy. The results of the Boruta method revealed that precipitation had the lowest mean importance at 5.8, while AET had the highest mean importance at 15.84. In contrast, the AET showed the highest importance for the sensitivity analysis of the groundwater suitability followed by the T_{min}, VPD, GWS, DEF, TWS, T_{max}, PET, precipitation, and runoff parameters, respectively (Supplementary material, Figure S14(b)).

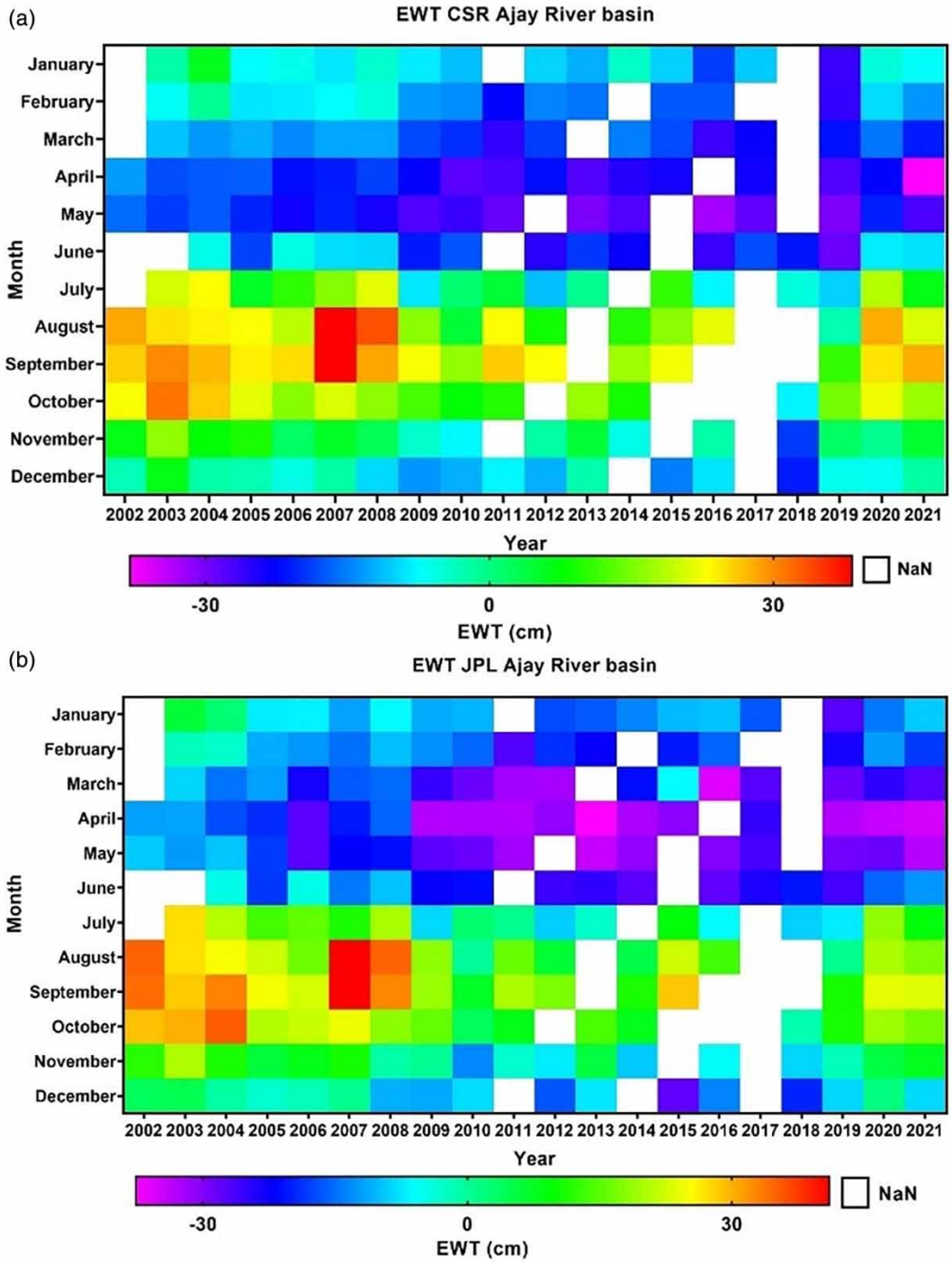

Figure 10 | Monthly equivalent water thickness (EWT) variation from 2002 to 2021 obtained by GRACE datasets: (a) Center for Space Research (CSR) and (b) Jet Propulsion Laboratory (JPL) in the Ajay River Basin.

4. DISCUSSION

Having a deep understanding of the various aspects of climatic variables that can affect natural resources is also important for effective environmental management. Therefore, climate change studies have a significant insights at the local level for reducing natural hazards. Salehie *et al.* (2022) assessed EWT for the water sustainability approach as more reliable through the GRACE and GLDAS v2.2 datasets. According to this approach, our study showed the early years has a high reliability of

Table 2 | OLS analysis results for hydrometeorological parameters

Parameters	β	ρ	Std err.
VPD	−0.4421	0.041	0.216
T_{max}	0.541	0.082	0.311
GWS	3.4739	0.000***	0.987
TWS	−3.1759	0.001**	0.95
T_{min}	0.8163	0.017*	0.95
Runoff	3.5603	0.000***	0.95
Precipitation	−2.1895	0.000***	0.95
PET	2.0466	0.000***	0.217
DEF	−3.9187	0.000***	0.217
AET	−2.6534	0.000***	0.217
Prob > $\chi^2 = 0.000$	$F = 1311$	$R^2 = 0.933$	Durbin–Watson = 1.396

β, coefficient; std. err., standard error; robust standard errors; F, statistical; R^2, linear regression.
*$p < 0.05$, **$p < 0.01$, and ***$p < 0.001$.

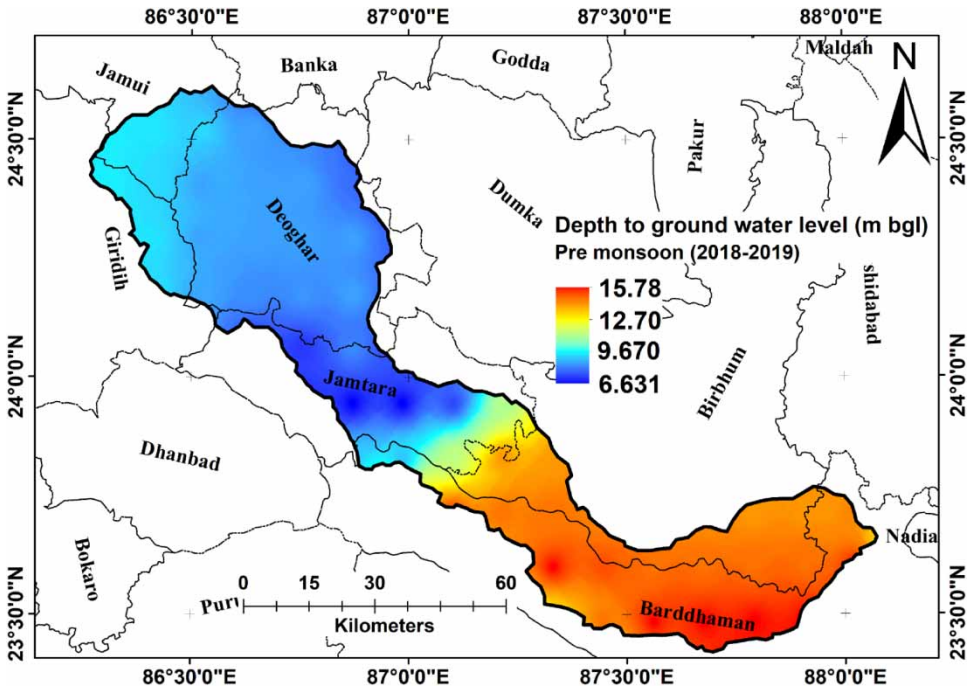

Figure 11 | The average depth to ground water level for the period of pre-monsoon, 2018–2019.

water resources during the pre-monsoon season. indicated less reliability in water sustainability, and vice versa. Dhar (2010) conducted a study on future (2040 and 2050) water availability and agricultural crop production in the context of climate change scenarios in the Ajay River Basin. Their research identified declining trends of precipitation, ET, soil moisture, and GWS in the southern part of West Bengal (Katwa and Gheropara). This outcome is comparable with the higher linear trend of the different climatic and hydrological variability in this region. The CMIP6 model provided quantitative insights into the potential impacts of the climate change cycle on future water storage conditions, droughts, and flood events from the upper to lower basins (Yang *et al.* 2020a, 2020b). In our study, the standardized TWS anomaly index helped identify drought-prone areas using hydrological datasets derived from GRACE and GLDAS. The findings indicate that the middle

Table 3 | Performances matrices of ML models

ML classifiers	Train accuracy	Test accuracy	Precision	Recall	F1 Score	AUROC
SVM	0.966	0.972	0.990	0.936	0.963	0.997
Naïve Bayes	0.951	0.944	0.905	0.955	0.929	0.994
Neural Net	0.951	0.948	0.913	0.955	0.933	0.998
Logistic Regression	0.958	0.951	0.921	0.955	0.938	0.998
QDA	0.963	0.955	0.908	0.982	0.943	0.995
CatBoost	0.970	0.976	0.972	0.964	0.968	0.995
Nearest Neighbors	0.990	0.986	0.982	0.982	0.982	0.995
Decision Tree	0.994	0.965	0.924	0.991	0.956	0.980
Random Forest	0.996	0.979	0.981	0.964	0.972	0.999
AdaBoost	0.999	0.986	0.973	0.991	0.982	0.999
XGBoost	0.999	0.986	0.973	0.991	0.982	0.991

Table 4 | Boruta feature importance analysis and selection of hydrometeorological parameters

Parameters	Mean importance	Median importance	Minimum importance	Maximum importance	Decision
VPD	15.22	14.98	14.2	16.42	Confirmed
T_{max}	13.59	13.47	12.97	14.82	Confirmed
GWS	14.48	14.57	12.72	16.73	Confirmed
TWS	13.97	13.92	12.32	15.37	Confirmed
T_{min}	15.38	15.36	14.21	16.76	Confirmed
Runoff	5.8	5.82	4.52	6.8	Confirmed
Precipitation	6.93	7.11	6.27	7.49	Confirmed
PET	10.41	10.36	9.86	11.1	Confirmed
DEF	14.4	14.32	13.72	15.68	Confirmed
AET	15.84	15.73	15.17	16.78	Confirmed

to upper regions of the river basin have very little water storage because of variations in precipitation and very significant groundwater level depletion as a result of human activity. Due to population pressure and extensive groundwater use for agriculture, one of the main issues is groundwater depletion. However, these datasets are valuable for implementing drought mitigation strategies in sustainable river basin planning (Deliry *et al.* 2022).

Based on the SAI of precipitation in the early years (2020), which showed low values, we observed a simultaneous high rate of DEF, and a declining trend in GWS and TWS in the southern most part of the area. The downstream portion of the river basin had an abundance of surface water, which resulted in significant water storage. The present work highlights that high runoff trends occur in the southern part (e.g., Gushkara, Gonna, Pratappur, Bhatkunda, Ausgram, Kurumba, Gopalpur, Bhedia, Debshala, and Basudha). These areas are primarily agrarian blocks in West Bengal and are characterized by high water consumption for domestic and agricultural purposes. Conversely, the variability and uncertainty of rainfall negatively impact irrigation scheduling as well as basin-scale groundwater discharge and recharge rates (Sahoo *et al.* 2021). Similarly, high DEF trends were observed in the middle part of the basin (e.g., Madhupur, Haripur, Lokepur, Sikandarpur, Amba, Charakamra, Banamalipur, Khajuri, Beniganj, Babuijore, and Chhotagholjor). Higher PET values are associated with higher temperatures in this study domain. Relative temperature leads to higher values of AET and PET across the region. Our research findings indicate a strong positive correlation between precipitation and runoff, AET, TWS, and GWS, while an inverse correlation exists with T_{max}, T_{min}, VPD, and DEF. A similar study on precipitation revealed significant effects at the $p < 0.05$ level with AET for river basin hydrology-related research (Desai *et al.* 2020).

Due to agricultural and hydrological droughts, the combined effects of TWS, GWS, precipitation, rising temperature, DEF, runoff, PET, and AET factors result in deteriorating climatic hydrological conditions throughout the research domain. Padhiary *et al.* (2019) reported that surface runoff and AET dynamics can determine the climate change adaptation and CRA status of the local livelihood condition. Furthermore, the low TWS and GWS trends are found in the northern part (i.e., Salaria, Patwabad, Rampur, Burhai, Dhamni, Kushaha, Madhupur, and Thari blocks) of the study area. Because groundwater is used for agriculture, the northern border of the region has a high groundwater stress zone due to strong trends in VPD, T_{max}, and T_{min} and low trends in precipitation. This region belongs to hard crystalline rocks (gneissic complex) that is abstracted negligible recharge for the GWS distribution (Banerjee *et al.* 2021). Chandra *et al.* (2019) showed that hard crystalline rocks with fracture networks are the major factors for steady sources of sustainable aquifer reserves. However, moderate TWS and GWS have occurred in the Bindapathar, Pahargara, Dimjuri, Geria, Pagla, Sima, Pindargaria, and Dalberia blocks of the basin. The majority of the basin area comprises agricultural land (57.54%) that required more irrigation and domestic purpose. Singha & Swain (2022) employed that water availability of the basin region is delineated by the land use pattern and hydrological condition that is strongly allied with climatic variability. Several studies reported that the lower part of the basin specified as more vulnerable to flood hazards that affect agricultural activity (Roy & Mistri 2016).

Moreover, this region is characterized by high TWS, GWS, and precipitation trends and moderate to low VPD, runoff, and DEF trends due to climate uncertainty. Climate change-induced severe floods and droughts have a definite impact on GWS and groundwater-dependent ecosystems (Swain *et al.* 2022). Our current study indicates a positive correlation between GWS, TWS, precipitation, AET, runoff, and an inverse correlation with temperature in the context of environmental and climate change studies (Sharma *et al.* 2022). The GWS, runoff, precipitation, PET, DEF, and AET are in good agreement of >99%; while TWS and T_{min} are <95% significance level for the groundwater resource availability of the study area. The statistical significance of the study's hydrological parameters for groundwater resource availability was evaluated using ML validation analysis. Groundwater level sampling locations were divided into a 70:30% ratio for ML model validation, with associated matrix evaluations. The OLS and Boruta feature importance methods were employed to minimize errors in climate-resilient strategies for this region (Lawal *et al.* 2023). The Boruta feature importance analysis highlighted that AET is highly sensitive in basin hydrology compared to runoff (Desai *et al.* 2020).

5. RECOMMENDATION FOR CLIMATE-RESILIENT AND CLIMATE-ADAPTATION STRATEGY

- The current study also highlights climate-resilient groundwater management strategies based on the United Nations' SDGs. We recommend that groundwater management and planning should incorporate ecosystem and biodiversity-based approaches, as well as community-driven adaptation solutions (Datta *et al.* 2022).
- Various long-term strategies and plans are needed to sustainably replenish groundwater resources, effectively turning them into drought reserves.
- It is important to consider the incorporation of climate models' projections, socio-economic factors, and hydrogeological aspects. Additionally, the use of multi-model scenarios should be prioritized instead of a single scenario or a single climate model (McDonald *et al.* 2022).
- A range of groundwater and agroecosystem-based sustainability approaches should be emphasized. These include securing ecological veracity, land use improvement, selecting suitable groundwater recharge sites, raising public awareness, purifying saline groundwater, recycling wastewater, improving groundwater recharge, promoting rainwater harvesting, implementing irrigation, and managing organic-plastic ponds and wetlands to build CRA strategy in the study area (Rao *et al.* 2019).
- Utilizing geospatial technology for micro-level planning, along with the creation of informative charts and maps, and engaging in cooperative community-based programs and workshops, early warning systems for weather forecasting, and initiatives like the Pradhan Mantri Krishi Sinchayee Yojana (PMKSY), Mahatma Gandhi National Rural Employment Guarantee Act (NREGA), and collaboration with NGOs should be promoted for surface and subsurface water conservation strategies (Samuel *et al.* 2022).
- In the northern part of the basin, the increasing number of water storage structures should be considered as part of groundwater resources management. These structures can be designed to regulate water flow and facilitate irrigation during severe droughts.
- Implementing climate-resilient and climate-smart agricultural practices, including crop rotation, diversification, mixed cropping, planting rescheduling, cropping pattern adjustments, irrigation scheduling, and micro-irrigation, can enhance rainfed agriculture systems for smallholder farmers.

- Encouraging afforestation and the adoption of water preservation actions can help reduce the AET, PET, soil erosion, and runoff losses in the basin. These measures can also help increase soil moisture storage as well as the TWS condition. Precision agricultural practices should be properly managed to ensure agricultural production can withstand the impacts of climate change.

6. CONCLUSIONS

The aim of the study was to understand the long-term spatiotemporal trends in hydrology (1958–2020), climatic (1958–2050), total water availability (2002–2021), and groundwater levels (2010–2017) changes. Various multi-satellite images, including TerraClimate, CMIP6, GRACE, GLDAS, MODIS, as well as *in situ* data from the CGWB of India (CGWB, India), were utilized to assess GWS in the Ajay river basin, India. The spatial trends of the SAI and SLR method were applied to analyze climatic and hydrologic trends. Projections from NEX GDDP CMIP6 SSP2-4.5, SSP5-8.5 and historical (i.e., MIROC6 and EC-Earth3) were used to examine future climate trends (2021–2050). The GRACE-derived JPL and CSR and GLDAS 2 CLM data were utilized for analyzing GWS, TWS, and EWT. Statistical correlation, OLS analysis, and Boruta sensitivity analysis were conducted to prioritize and understand the relationships among the observed parameters. The study found that GRACE-derived EWT measurements in recent years have indicated a reduction in water resource reliability, suggesting a declining trend in post-monsoon periods. Linear trends in annual precipitation and T_{max} values ranged from −0.04 to 0.10 mm/year and 0.005–0.007 °C, respectively. Additionally, TWS and GWS exhibited higher values in the southern part compared to the northern part. A declining trend in TWS was observed in the northern part, while a high GWS value was noted in the southern part. In 2020, early-time precipitation, AET, runoff, TWS, and GWS were concentrated at lower levels in the southern region, whereas T_{max}, T_{min}, PET, VPD, and DEF exhibited inverse conditions in this region. The study's findings underscore the direct impact of climate uncertainty on the vulnerability of agricultural productivity in the north-western part of the region. These findings also offer insights into various climate resilience practices that can be applied to sustainable agriculture. However, further research is needed to comprehensively assess the potential impacts of climate change on groundwater practices among smallholder farmers and households by considering cultural and behavioral aspects of the local community. Also, we implemented the meteorological forcing datasets for improvement of the CRA adoption strategy. Different stakeholders' perceptions, and community involvement are considered for the CRA. Future studies are explored to encompass the findings of the current study to a superior range of environments crossways the globe. The study's reported observed data shortage issues and inadequate field validation are its drawbacks.

ACKNOWLEDGEMENTS

The authors are grateful to the TerraClimate, United States Geological Survey (USGS), and the ESA, GEE and CGWB for providing the required hydroclimate, satellite images, and groundwater level data. We acknowledge the project 'Integration of Digital Augmentation for sustainable Agroecosystem in Western Lateritic Zone under National Hydrology Project, West Bengal' under which this work is mapped. The author also thanks the International Center for Agricultural Research in the Dry Areas (ICARDA) for providing necessary support for this research work. The authors are also grateful to editors and potential reviewers.

AUTHORS' CONTRIBUTIONS

S.S., C.S., and A.G. were involved in conceptualization; S.S., C.S., and A.G. prepared the methodology; S.S., C.S., and A.G. did software analysis; S.S., C.S., and A.G. validated the study; S.S., C.S., and A.G. did formal analysis; S.S., C.S., and A.G. investigated the study; S.S., C.S., and A.G. collected resources; S.S. and C.S. did data creation; S.S., C.S. A.G., and B.P. were involved in writing – original draft preparation; S.A., T.H.A., S.S., C.S., A.G., H.G.A., A.R.M.T.I., and B.P. did writing – review and editing; A.G. and H.G.A. acquired funding. All authors have read and agreed to the published version of the manuscript.

DATA AVAILABILITY STATEMENT

Data cannot be made publicly available; readers should contact the corresponding author for details.

CONFLICT OF INTEREST

The authors declare there is no conflict.

REFERENCES

Acevedo, M., Pixley, K., Zinyengere, N., Meng, S., Tufan, H., Cichy, K., Bizikova, L., Isaacs, K., Ghezzi-Kopel, K. & Porciello, J. 2020 A scoping review of adoption of climate-resilient crops by small-scale producers in low-and middle-income countries. *Nat. Plants* **6** (10), 1231–1241.

Amiri, M. A. & Gocic, M. 2021 Analyzing the applicability of some precipitation concentration indices over Serbia. *Theor. Appl. Climatol.* **146**, 645–656. https://doi.org/10.1007/s00704-021-03743-5.

Amiri, M. A. & Gocic, M. 2023 Analysis of temporal and spatial variations of drought over Serbia by investigating the applicability of precipitation-based drought indices. *Theor. Appl. Climatol.* **154**, 261–274. https://doi.org/10.1007/s00704-023-04554-6.

Araghi, A., Martinez, C. J. & Adamowski, J. F. 2023 Evaluation of TerraClimate gridded data across diverse climates in Iran. *Earth Sci. Inf.* **16**, 1347–1358. https://doi.org/10.1007/s12145-023-00967-z.

Arneth, A., Denton, F., Agus, F., Elbehri, A., Erb, K., Osman Elasha, B., Rahimi, M., Rounsevell, M., Spence, A. & Valentini, R., 2019 Framing and Context. In: *Climate Change and Land: An IPCC Special Report on Climate Change, Desertification, Land Degradation, Sustainable Land Management, Food Security, and Greenhouse gas Fluxes in Terrestrial Ecosystems* (Shukla, P.R., Skea, J., Calvo Buendia, E., Masson-Delmotte, V., Pörtner, H.-O., Roberts, D.C., Zhai, P., Slade, R., Connors, S., van Diemen, R., Ferrat, M., Haughey, E., Luz, S., Neogi, S., Pathak, M., Petzold, J., Portugal Pereira, J., Vyas, P., Huntley, E., Kissick, K., Belkacemi, M. & Malley, J., eds). Cambridge University Press, Cambridge, United Kingdom; New York, NY, USA, p. 1535.

Banerjee, M., Ghosh, D. & Mandal, M. 2021 Analysis of current direction in a tropical fluvial system: A study of Ajay river basin within West Bengal, India. *J. Earth Syst. Sci.* **130**. https://doi.org/10.1007/s12040-020-01520-y.

Bhattacharya, A. K., 1972 A study of the Ajay river sediments. In: *The Bhagirathi–Hooghly Basin: Proceedings of the Interdisciplinary Symposium* (Bagchi K, G. & Kanjilal, S., eds). Sri Sibendranath Kanjilal, Calcutta, pp. 18–32.

Bherea, S. & Reddy, M. J. 2022 Assessment of reliability, resilience, and vulnerability (RRV) of terrestrial water storage using gravity recovery and climate experiment (GRACE) for Indian river basins. *Remote Sens. Appl. Soc. Environ.* **28**, 100851. https://doi.org/10.1016/j.rsase.2022.100851.

Bilginola, K., Denlia, H. H. & Zafer ùekera, D. 2015 Ordinary least squares regression method approach for site selection of Automated Teller Machines (ATMs). *Proc. Environ. Sci.* **26**, 66–69.

Breiman, L. 2001 Random forests. *Mach. Learn.* **45** (1), 5–32. doi:10.1023/A:1010933404324.

Caretta, M. A., Mukherji, A., Arfanuzzaman, M., Betts, R. A., Gelfan, A., Hirabayashi, Y., Lissner, T. K., Liu, J., Lopez Gunn, E., Morgan, R., Mwanga, S. & Supratid, S., 2022 Water. In: *Climate Change 2022: Impacts, Adaptation and Vulnerability. Contribution of Working Group II to the Sixth Assessment Report of the Intergovernmental Panel on Climate Change* (Pörtner, H. O., Roberts, D. C., Tignor, M. M. B., Poloczanska, E., Mintenbeck, K., Alegria, A., Craig, M., Langsdorf, S., Löschke, S., Möller, V., Okem, A. & Rama, B. eds). Cambridge University Press, Cambridge, UK; New York, NY, USA, pp. 551–712. doi:10.1017/9781009325844.006.

Chandra, S., Auken, E., Maurya, P. K., Ahmed, S. & Verma, S. K. 2019 Large scale mapping of fractures and groundwater pathways in crystalline hardrock By AEM. *Sci. Rep.* **9** (1). doi:10.1038/s41598-018-36153-1.

Chen, T. & Guestrin, C. 2016 *XGBoost: A Scalable Tree Boosting System*. KDD '16: Proceedings of the 22nd ACM SIGKDD International Conference on Knowledge Discovery and Data Mining, San Francisco California USA, pp. 785–794. https://doi.org/10.1145/2939672.2939785

Cortes, C. & Vapnik, V. 1995 Support-vector networks. *Mach. Learn.* **20**, 273–297.

Datta, P., Behera, B. & Rahut, D. B. 2022 Climate change and Indian agriculture: A systematic review of farmers' perception, adaptation, and transformation. *Environ. Challenges* **8**. https://doi.org/10.1016/j.envc.2022.100543.

Deliry, S. I., Pekkan, E. & Avdan, U. 2022 GIS-based water budget estimation of the Kizilirmak River Basin using GLDAS-2.1 Noah and CLSM models and remote sensing observations. *J. Indian Soc. Remote Sens.* **50**, 1191–1209.

Desai, S., Singh, D. K., Islam, A. & Sarangi, A. 2020 Impact of climate change on the hydrology of a semi-arid river basin of India under hypothetical and projected climate change scenarios. *J. Water Clim. Change* **12** (3), 969–996. jwc2020287. doi:10.2166/wcc.2020.287.

Dhar, S. 2010 Investigation into the effects of climate change for the Ajay River Basin using hydroinformatics. *J. Manage. Public Policy* **2**, 1.

Dhar, A., Sahoo, S., Dey, S. & Sahoo, M. 2014 Evaluation of recharge and groundwater dynamics of a shallow alluvial aquifer in central ganga basin, Kanpur (India). *Nat. Resour. Res.* **23**, 409–422.

Filgueiras, R., Venancio, L. P., Aleman, C. C. & Cunha, F. F. D. 2022 Comparison and calibration of terraclimate climatological variables over the Brazilian territory. *J. South Am. Earth Sci.* **117**, 103882. https://doi.org/10.1016/j.jsames.2022.103882.

Freund, Y. & Schapire, R. E. 1995 A decision-theoretic generalization of on-line learning and an application to boosting. In: Vitányi, P. (eds) Computational Learning Theory. *EuroCOLT 1995. Lecture Notes in Computer Science*, vol. 904. Springer, Berlin, Heidelberg. https://doi.org/10.1007/3-540-59119-2_166.

Geological Survey of India (GSI). 1985 *Quaternary Geological and Geomorphological Mapping and Geoscientific Studies of Ajay Basin, West Bengal for Assessment of Land and Water Resources; Unpublished Progress Report, Regional Geology Division-I, Eastern Region, Calcutta*.

Guptha, G. C., Swain, S., Al-Ansari, N., Taloor, A. K. & Dayal, D. 2022 Assessing the role of SuDS in resilience enhancement of urban drainage system: A case study of Gurugram City India. *Urb. Clim.* **41**, 101075. https://doi.org/10.1016/j.uclim.2021.101075.

Hidalgo-García, D. & Arco-Díaz, J. 2022 Modeling the Surface Urban Heat Island (SUHI) to study of its relationship with variations in the thermal field and with the indices of land use in the metropolitan area of Granada (Spain). *Sustain. Cities Soc.* **87**, 104166. https://doi.org/10.1016/j.scs.2022.104166.

India Meteorological Department (IMD). 2018 *Purchased Climatic Data*. IMD, Pune, India.

IPCC 2013 Climate Change 2013: The Physical Science Basis. In: *Working Group I Contribution to the Fifth Assessment Report of the Intergovernmental Panel on Climate Change* (Stocker, T.F., Qin, D., Plattner, G. K., Tignor, M., Allen, S.K., Boschung, J., Nauels, A., Xia, Y., Bex, V., & Midgley, P.M. eds). Cambridge University Press, Cambridge, United Kingdom; New York, NY, USA, p. 1535.

IPCC 2019 Summary to Policymakers. In: *Climate Change and Land: An IPCC Special Report on Climate Change, Desertification, Land Degradation, Sustainable Land Management, Food Security, and Greenhouse Gas Fluxes in Terrestrial Ecosystems* (Shukla, P. R., Skea, J., Calvo Buendia, E., Masson-Delmotte, V., Pörtner, H.O., Roberts, D. C., Zhai, P., Slade, R., Connors, S., van Diemen, R., Ferrat, E. Haughey, S. Luz, S. Neogi, M. Pathak, J. Petzold, J. Portugal Pereira, P. Vyas, E. Huntley, K. Kissick, M., Belkacemi, M. & Malley, J. eds). IPCC, Cambridge University Press, Cambridge.

Kadavi, P. R., Lee, C.-W. & Lee, S. 2019 Landslide-susceptibility mapping in Gangwon-do, South Korea, using logistic regression and decision tree models. *Environ. Earth Sci.* **78**, 116.

Karan, K., Singh, D., Singh, P. K., Bharati, B., Singh, T. P. & Berndtsson, R. 2022 Implications of future climate change on crop and irrigation water requirements in a semi-arid river basin using CMIP6 GCMs. *J. Arid Land* **14**, 1234–1257. https://doi.org/10.1007/s40333-022-0081-1.

Kendall, M. G. 1975 *Rank Correlation Methods*. Griffin, London, UK.

Kim, D., Chun, J. A. & Choi, S. J. 2019 Incorporating the logistic regression into a decision-centric assessment of climate change impacts on a complex river system. *Hydrol. Earth Syst. Sci.* **23**, 1145–1162. https://doi.org/10.5194/hess-23-1145-2019.

Koudahe, K., Kayode, A. J., Samson, A. O., Adebola, A. A. & Djaman, K. 2017 Trend analysis in standardized precipitation index and standardized anomaly index in the context of climate change in Southern Togo. *Atmos. Clim. Sci.* **7**, 401–423. https://doi.org/10.4236/acs.2017.74030.

Kumar, M., Raghuwanshi, N., Singh, R., Wallender, W. & Pruitt, W. 2002 Estimating evapotranspiration using artificial neural network. *J. Irrig. Drain. Eng.* **128**, 224–233.

Lawal, I. M., Bertram, D., White, C. J., Kutty, S. R. M., Hassan, I. & Jagaba, A. H. 2023 Application of Boruta algorithms as a robust methodology for performance evaluation of CMIP6 general circulation models for hydro-climatic studies. *Theor. Appl. Climatol.* **153**, 113–135. https://doi.org/10.1007/s00704-023-04466-5.

Mann, H. B. 1945 Nonparametric tests against trend. *Econometrica* **13**, 245–259.

McDonald, A. J., Balwinder-Singh, Keil, A., Srivastava, A., Craufurd, P., Kishore, A., Kumar, V., Paudel, G., Singh, S., Singh, A. K., Sohane, R. K. & Malik, R. K. 2022 Time management governs climate resilience and productivity in the coupled rice–wheat cropping systems of eastern India. *Nat. Food* **3**, 542–551. https://doi.org/10.1038/s43016-022-00549-0.

Milan, G. & Amiri, M. A. 2023 Analysis of spatial variability and patterns of drought. In: *Integrated Drought Management* (Singh, V. P., Jhajharia, D. & Mirabbasi, R. (eds)). Vol. 2, CRC Press, pp. 31–42. doi:10.1201/9781003276548-3.

Mushtaq, M. S. & Mellouk, A. 2017 Methodologies for subjective video streaming QoE assessment. In: *Quality of Experience Paradigm in Multimedia Services*. Application to OTT Video Streaming and VoIP Services. Mushtaq, M. S. & Mellouk, A. (eds). pp. 27–57. https://doi.org/10.1016/B978-1-78548-109-3.50002-3

Niyogi, M. 1988 Spatio-temporal analysis of run-off in the Ajay basin. *Geogr. Rev. India* **50** (2), 58–66.

Padhiary, J., Patra, K. C., Dash, S. S. & Uday, K. A. 2019 Climate change impact assessment on hydrological fluxes based on ensemble GCM outputs: A case study in eastern Indian River Basin. *J. Water Clim. Change* **11** (4), 1676–1694. jwc2019080. doi:10.2166/wcc.2019.080.

Pekel, J. F., Cottam, A., Gorelick, N. & Belward, A. S. 2016 High-resolution mapping of global surface water and its long-term changes. *Res. Lett.*, 1–5. doi:10.1038/nature20584.

Prokhorenkova, L., Gusev, G., Vorobev, A., Dorogush, A. V. & Gulin, A. 2018 Catboost: Unbiased boosting with categorical features. *Adv. Neural Inf. Process. Syst.* **31**, 1–11.

Pushpanjali, S., Josily, C. A., Rama, K., Raju, B. & Karthikeyan, K. 2021 Spatial estimation and climate projected change of covermanagement factor in semi-arid region of India. *Indian J. Agric. Sci* **4**, 521–525.

Qin, Y. 2018 A review of quadratic discriminant analysis for high-dimensional data. *WIREs Comput. Stat.* **10** (4), e1434. https://doi.org/10.1002/wics.1434.

Rao, C. S., Kareemulla, K., Krishnan, P., Murthy, G. R. K., Ramesh, P., Ananthan, P. S. & Joshi, P. K. 2019 Agro-ecosystem based sustainability indicators for climate resilient agriculture in India: A conceptual framework. *Ecol. Indic.* **105**, 621–633.

Roy, S. & Mistri, B. 2016 Flooding in the confluence zone of the Ajay and the Kunur Rivers, West Bengal: A hydrogeomorphological assessment. *J. Indian Geomorphology* **4**, 73–83. ISSN 2320-0731.

Rusia, D. K., Swain, K. C. & Singha, C. 2018 Integrated geospatial technique for potential groundwater zone (PGZ) identification. *J. Agroecol. Nat. Resour. Manage.* **5** (3), 142–150.

Sahoo, S. & Govind, A. 2023 Understanding changes in the hydrometeorological conditions towards climate-resilient agricultural interventions in Ethiopia. *Agronomy* **13** (2), 387.

Sahoo, S., Swain, S., Goswami, A., Sharma, R. & Pateriya, B. 2021 Assessment of trends and multi-decadal changes in groundwater level in parts of the Malwa region, Punjab India. *Groundwater Sustainable Dev.* **14**, 100644. https://doi.org/10.1016/j.gsd.2021.100644.

Salehie, O., Ismail, T. B., Shahid, S., Hamed, M. M., Chinnasamy, P. & Wang, X. 2022 Assessment of water resources availability in Amu Darya River Basin using GRACE data. *Water* **14**, 533. https://doi.org/10.3390/w14040533.

Sam, A. S., Padmaja, S. S., Kachele, H., Kumar, R. & Muller, K. 2020 Climate change, drought and rural communities: Understanding people's perceptions and adaptations in rural eastern India. *Int. J. Disaster Risk Reduct.* **44**, 101436.

Samuel, J., Rao, C. A. R, Raju, B. M. K., Reddy, A. G. K., Kumar, R. N., Osman, M., Singh, V. K. & Prasad, J. V. N. S. 2022 Assessing the impact of climate resilient technologies in minimizing drought impacts on farm incomes in drylands. *Sustainability* **14**, 382. https://doi.org/10.3390/su14010382.

Sharma, A., Maharana, P., Sahoo, S. & Sharma, P. 2022 Environmental change and groundwater variability in South Bihar, India. *Groundwater Sustainable Dev.* **19**, 100846.

Singh, S. 2020 Farmers' perception of climate change and adaptation decisions: A micro-level evidence from Bundelkhand Region, India. *Ecol. Indic* **116**, 106475. doi:10.1016/j.ecolind.2020.106475.

Singha, C. & Swain, K. C. 2022 *Using Earth Observations and GLDAS Model to Monitor Water Budgets for River Basin Management*. Springer, Singapore, p. 176. https://doi.org/10.1007/978-981-16-4629-4_34.

Singha, C., Swain, K. C. & Swain, S. K. 2020 Best crop rotation selection with GIS-AHP technique using soil nutrient variability. *Agriculture* **10**, 213. https://doi.org/10.3390/agriculture10060213.

Singha, C., Swain, K. C., Meliho, M., Abdo, H. G., Almohamad, H. & Al-Mutiry, M. 2022 Spatial analysis of flood hazard zoning map using novel hybrid machine learning technique in Assam, India. *Remote Sens.* **14**, 6229. https://doi.org/10.3390/rs14246229.

Swain, S., Taloor, A. K., Dhal, L., Sahoo, S. & Al-Ansari, N. 2022 Impact of climate change on groundwater hydrology: A comprehensive review and current status of the Indian hydrogeology. *Appl. Water Sci.* **12**, 120. https://doi.org/10.1007/s13201-022-01652-0.

Tatebe, H., Ogura, T., Nitta, T., Komuro, Y., Ogochi, K., Takemura, T., Sudo, K., Sekiguchi, M., Abe, M., Saito, F., Chikira, M., Watanabe, S., Mori, M., Hirota, N., Kawatani, Y., Mochizuki, T., Yoshimura, K., Takata, K., O'ishi, R., Yamazaki, D., Suzuki, T., Kurogi, M., Kataoka, T., Watanabe, M. & Kimoto, M. 2019 Description and basic evaluation of simulated mean state, internal variability, and climate sensitivity in MIROC6. *Geosci. Model Dev.* **12**, 2727–2765. https://doi.org/10.5194/gmd-12-2727-2019.

Werners, S. E., Werners, S. E., Sparkes, E., Totin, E., Abeld, N., Bhadwal, S., Butler, J. R. A., Douxchamps, S., James, H., Methner, N., Siebeneck, J., Stringer, L. C., Vincent, K., Wise, R. M. & Tebboth, M. G. L. 2021 Advancing climate resilient development pathways since the IPCC's fifth assessment report. *Environ. Sci. Policy* **126**, 168–176.

Yang, P., Zhang, Y., Xia, J. & Sun, S. 2020a Investigation of precipitation concentration and trends and their potential drivers in the major river basins of Central Asia. *Atmos. Res.* **245**, 105128. https://doi.org/10.1016/j.atmosres.2020.105128.

Yang, Q., Gao, C., Zha, Q. & Zhang, P. 2020b Changes of climate and runoff under the representative concentration pathways scenarios in the upper reaches of the Huaihe River. *J. Anhui Agric. Sci.* **48** (3), 209–214.

Zhang, M. L. & Zhou, Z. H. 2007 ML-KNN: A lazy learning approach to multi-label learning. *Pattern Recognit.* **40** (7), 2038–2048.

First received 22 September 2023; accepted in revised form 4 December 2023. Available online 15 December 2023